International Journal of
Molecular Sciences

MDPI

Article

Hyperbilirubinemia in Gunn Rats Is Associated with Decreased Inflammatory Response in LPS-Mediated Systemic Inflammation

Petra Valaskova [1], Ales Dvorak [1], Martin Lenicek [1], Katerina Zizalova [1], Nikolina Kutinova-Canova [2], Jaroslav Zelenka [3], Monika Cahova [4], Libor Vitek [1,5] and Lucie Muchova [1,*]

1 Institute of Medical Biochemistry and Laboratory Diagnostics, First Faculty of Medicine, Charles University and General University Hospital in Prague, 12108 Prague, Czech Republic; petra.valaskova@lf1.cuni.cz (P.V.); aleshdvorak@gmail.com (A.D.); mleni@centrum.cz (M.L.); katka.ziza@seznam.cz (K.Z.); vitek@cesnet.cz (L.V.)
2 Institute of Pharmacology, First Faculty of Medicine, Charles University and General University Hospital in Prague, 12800 Prague, Czech Republic; Nikolina.Canova@lf1.cuni.cz
3 Department of Biochemistry and Microbiology, University of Chemistry and Technology, 16628 Prague, Czech Republic; jar.zelenka@gmail.com
4 Department of Experimental Diabetology, Institute of Clinical and Experimental Medicine, 14021 Prague, Czech Republic; moca@ikem.cz
5 4th Department of Medicine—Department of Gastroenterology and Hepatology, First Faculty of Medicine, Charles University and General University Hospital in Prague, 12808 Prague, Czech Republic
* Correspondence: lucie.muchova@lf1.cuni.cz; +420-224964199

Received: 15 April 2019; Accepted: 4 May 2019; Published: 9 May 2019

Abstract: Decreased inflammatory status has been reported in subjects with mild unconjugated hyperbilirubinemia. However, mechanisms of the anti-inflammatory actions of bilirubin (BR) are not fully understood. The aim of this study is to assess the role of BR in systemic inflammation using hyperbilirubinemic Gunn rats as well as their normobilirubinemic littermates and further in primary hepatocytes. The rats were treated with lipopolysaccharide (LPS, 6 mg/kg intraperitoneally) for 12 h, their blood and liver were collected for analyses of inflammatory and hepatic injury markers. Primary hepatocytes were treated with BR and TNF-α. LPS-treated Gunn rats had a significantly decreased inflammatory response, as evidenced by the anti-inflammatory profile of white blood cell subsets, and lower hepatic and systemic expressions of IL-6, TNF-α, IL-1β, and IL-10. Hepatic mRNA expression of LPS-binding protein was upregulated in Gunn rats before and after LPS treatment. In addition, liver injury markers were lower in Gunn rats as compared to in LPS-treated controls. The exposure of primary hepatocytes to TNF-α with BR led to a milder decrease in phosphorylation of the NF-κB p65 subunit compared to in cells without BR. In conclusion, hyperbilirubinemia in Gunn rats is associated with an attenuated systemic inflammatory response and decreased liver damage upon exposure to LPS.

Keywords: bilirubin; Gunn rats; hyperbilirubinemia; inflammation; LPS; NF-κB

1. Introduction

Bilirubin (BR), the end product of the heme degradation pathway in the intravascular compartment, is an important endogenous antioxidant, and it plays a crucial role in protection against oxidative stress as has been demonstrated in numerous in vitro, in vivo, and clinical studies (for review, see [1]). Recently, it has been shown that BR exerts potent anti-inflammatory and immunomodulatory activities [2]. In fact, mild hyperbilirubinemia has been associated with a reduced risk of diseases linked to increased oxidative stress and chronic inflammation (for review, see [3]).

A wide array of BR anti-inflammatory effects are mediated by multiple mechanisms, and indeed, BR is capable of modulating all stages of both the innate as well as the adaptive immune system [2]. These, predominantly suppressing activities, are aimed against: the complement system [4], damage-associated molecular patterns (DAMPs) signaling [5], Toll-like receptors (TLRs), such as TLR4 (a bacterial lipopolysaccharide (LPS) receptor) [6], macrophage activities [7] as well as B cell-mediated antibody production [8], and differentiation of T cells, including regulatory T cells (Tregs) [9], all with wide-spread potential clinical consequences towards autoimmune diseases [10] and transplant medicine [5,9].

An increasing body of evidence suggests that mildly elevated BR concentrations could suppress production of pro-inflammatory cytokines [5,10,11]. The secretion of cytokines is under the control of nuclear factor kappa B (NF-κB), a master regulator of numerous genes involved in the immune and inflammatory responses [12]. In the canonical pathway, NF-κB is activated by many signals including bacterial LPS, which binds to the LPS-binding protein (LBP), and then interacts with TLR4/CD14 receptors [13]. In resting cells, NF-κB is inactive, located in the cytoplasm bound to its inhibitor IκB. Upon activation, the IκB kinase (IKK) complex activates NF-κB by phosphorylating IκB, resulting in ubiquitination and proteasome degradation of IκB. Active NF-κB then translocates into the nucleus and activates specific genes [14]. Taking into consideration the reported inhibitory effects of BR on protein phosphorylation [15] as well as its general immune system-suppressing activities [10], we hypothesize that BR might also interfere with phosphorylation of NF-κB p65 subunit, and thus prevent translocation of NF-κB into the nucleus.

Therefore, the aim of our study was thus to evaluate the pathophysiological role of BR in LPS-induced inflammation in hyperbilirubinemic Gunn rats and primary hepatocytes isolated from hyper- and normobilirubinemic animals.

2. Results

2.1. Hyperbilirubinemia in Gunn Rats Is Associated with Decreased Systemic Inflammatory Response in LPS-Induced Sepsis

To evaluate the effect of BR on systemic and hepatic inflammation, the complete blood count, as well as serum markers of liver injury, was measured in hyperbilirubinemic Gunn rats as well as in their normobilirubinemic heterozygous littermates. Interestingly, higher white blood cell (WBC) counts were observed after LPS treatment in control rats as compared to in hyperbilirubinemic Gunn animals ($(12.39 \pm 5.26) \times 10^9$/L vs. $(8.70 \pm 1.94) \times 10^9$/L, $p = 0.05$). Following LPS administration, significant increases were detected in the proportions of neutrophils (396 ± 301%, $p < 0.01$), monocytes (565 ± 242%, $p < 0.01$), basophils (338 ± 271%, $p < 0.05$), as well as eosinophils (448 ± 419%, $p < 0.05$), together with a decrease in the lymphocyte count (up to 23 ± 13%, $p < 0.01$) in control animals. However, these changes were substantially attenuated in hyperbilirubinemic Gunn rats (Figure 1a–f).

Simultaneously, marked changes in the $CD4^+/CD8^+$ T cells were observed in both hyperbilirubinemic Gunn rats and control animals upon exposure to LPS. In fact, the $CD4^+/CD8^+$ T ratio, a marker of immune activation [16], was 13 times higher in hyperbilirubinemic Gunn rats as compared to in controls ($p < 0.05$) (Figure 1g,h).

To evaluate the effect of hyperbilirubinemia on mediators of systemic inflammation, we first measured mRNA expression of the selected cytokines in the liver tissue as well as in the WBC of control and LPS-treated animals. The lower expressions of liver pro-inflammatory cytokines interleukin-6 (*IL-6*) (50 ± 49%, $p < 0.05$) and tumor necrosis factor-α (*TNF-α*) (59 ± 26%, $p < 0.05$) were observed in Gunn rat livers without LPS treatment compared to those in heterozygous littermates. After LPS administration, significantly lower increases in pro-inflammatory *TNF-α* (34 ± 21%, $p < 0.05$), interleukin-1β (*IL-1β*) (57 ± 30%, $p < 0.05$), and anti-inflammatory interleukin-10 (*IL-10*) (40 ± 22%, $p < 0.05$, Figure 2a–d) were detected in Gunn rats as compared to in normobilirubinemic controls 12 h after saline or LPS administration. Similar results in mRNA cytokine expressions were observed also in the WBC. Indeed, the elevation levels of cytokines *IL-6*, *TNF-α*, *IL-1β* and *IL-10* after LPS administration were significantly

attenuated in Gunn rats (49 ± 35%, 43 ± 43%, 31 ± 28%, and 24 ± 13%, respectively, $p < 0.05$) compared to that in control animals (Figure 2e–h).

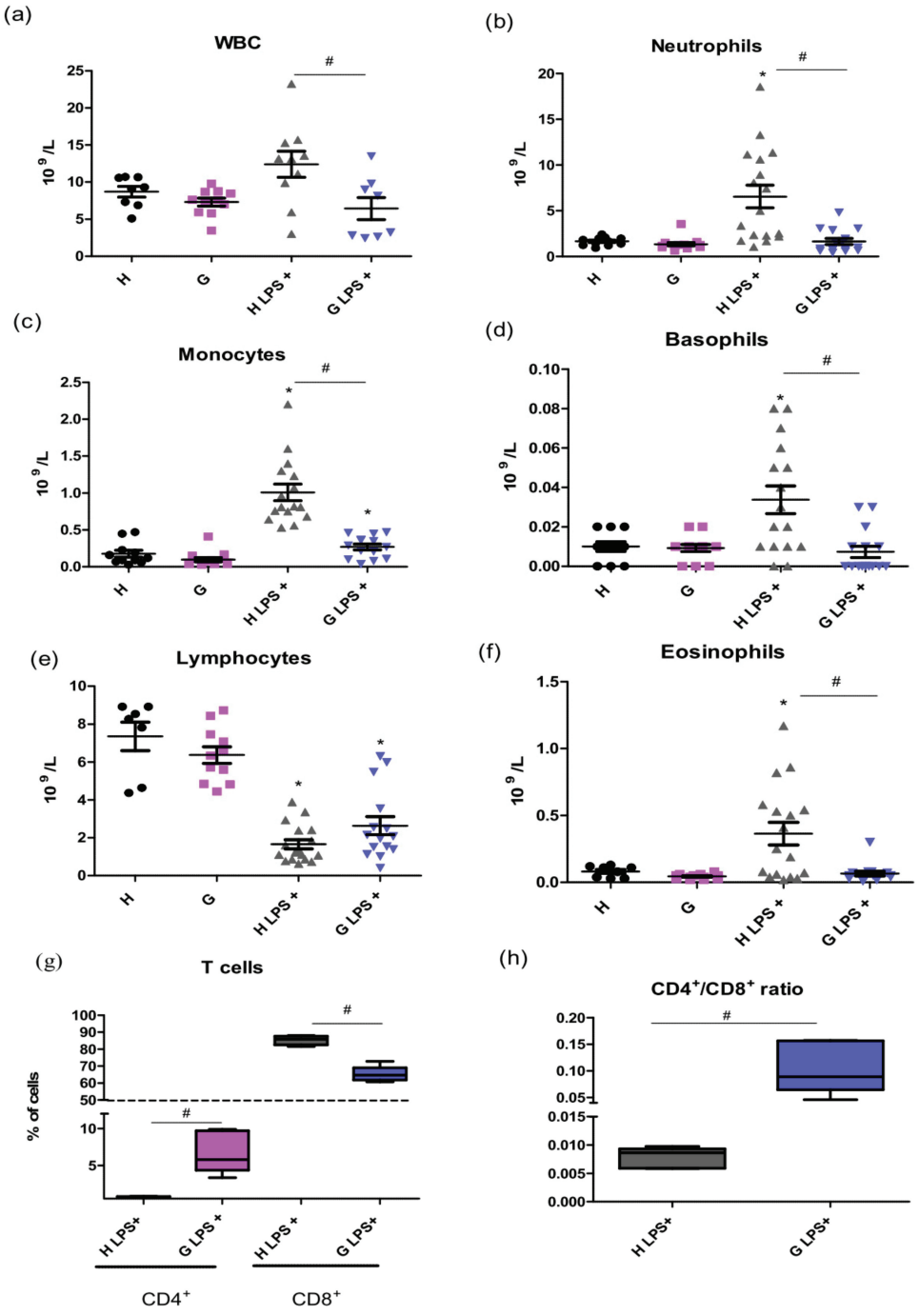

Figure 1. The effect of LPS-induced inflammation on WBC in hyperbilirubinemic Gunn rats. Total WBC cells (**a**) and their subpopulations (**b**–**f**) including T cells count (**g**) and $CD4^+/CD8^+$ ratio (**h**) were measured 12 h after LPS administration (6 mg/kg i.p.) in normobilirubinemic heterozygous controls (H or H LPS+) and hyperbilirubinemic Gunn rats (G or G LPS+), respectively. * $p < 0.05$ vs. corresponding control, # $p < 0.05$ vs. LPS-treated group. $n = 8$ animals per group (minimum).

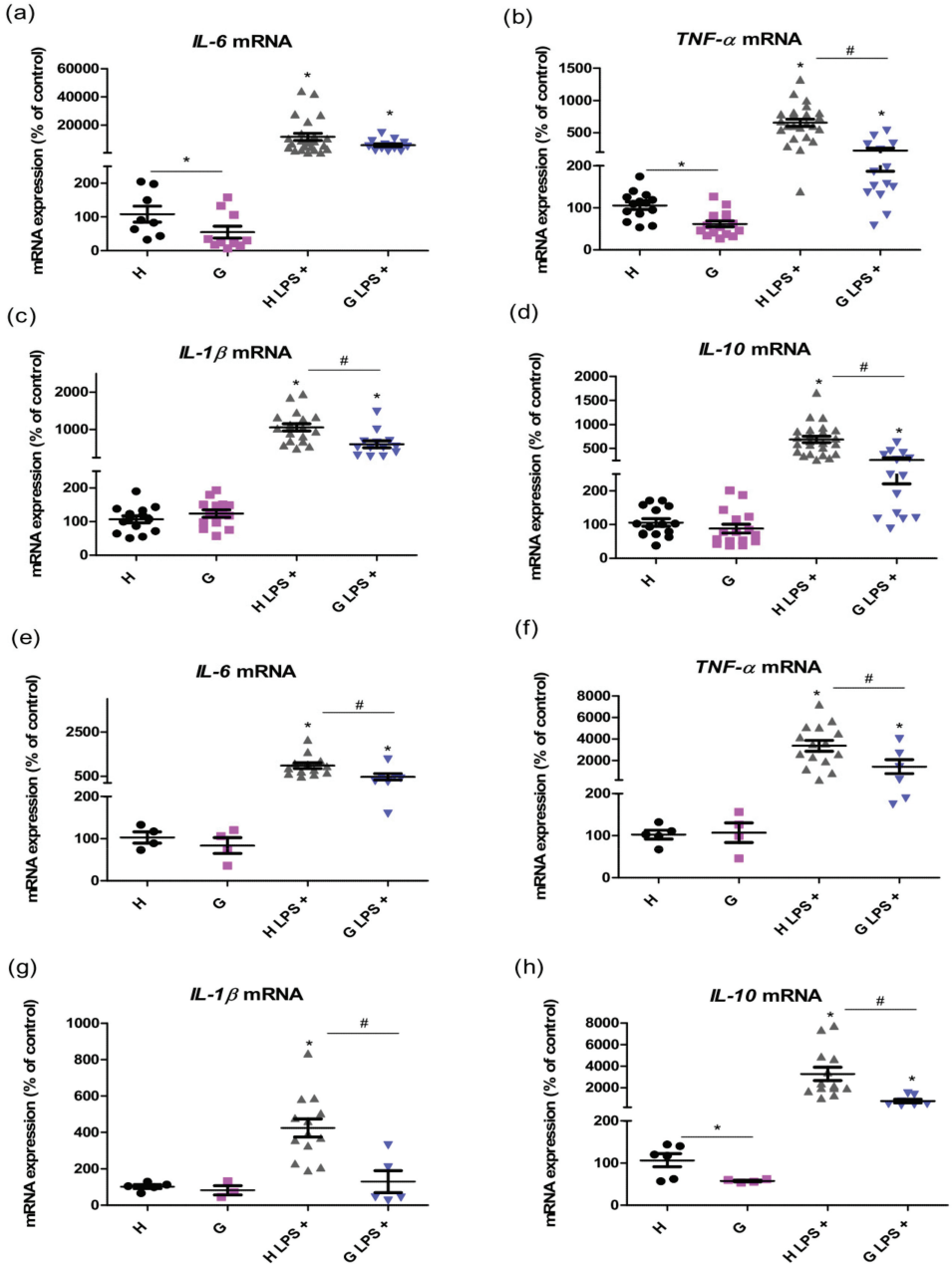

Figure 2. The effects of LPS-induced inflammation on mRNA cytokine expression in the liver and WBC of hyperbilirubinemic Gunn rats. mRNA expressions of pro- and anti-inflammatory cytokines *IL-6*, *TNF-α*, *IL-1β*, and *IL-10* were measured in the liver tissue (**a**–**d**) and white blood cells (**e**–**h**) 12 h after saline or LPS administration (6 mg/kg i.p.) in normobilirubinemic heterozygous controls (H or H LPS+) and hyperbilirubinemic Gunn rats (G or G LPS+), respectively. * $p < 0.05$ vs. corresponding control, # $p < 0.05$ vs. LPS-treated group. $n = 5$ animals per group (minimum).

Serum concentrations of selected cytokines were measured to confirm the functional translation of their mRNA expressions. In untreated animals, the concentrations of all tested cytokines were under the limit of detection. However, after LPS treatment, the changes in concentrations of most cytokines followed the pattern of mRNA expressions (although the concentration of IL-1β was under the limit of detection). Compared to that of controls, lower concentrations of IL-6 (35 ± 1%) as well as those of TNF-α (60 ± 56%) and IL-10 (25 ± 23%, $p < 0.05$) were observed in Gunn rats exposed to LPS (Figure 3). This data resulted in a marked difference in the IL-10/TNF-α ratio, a marker of immune homeostasis, between H LPS+ and G LPS+ experimental groups (0.51:0.19, $p < 0.05$).

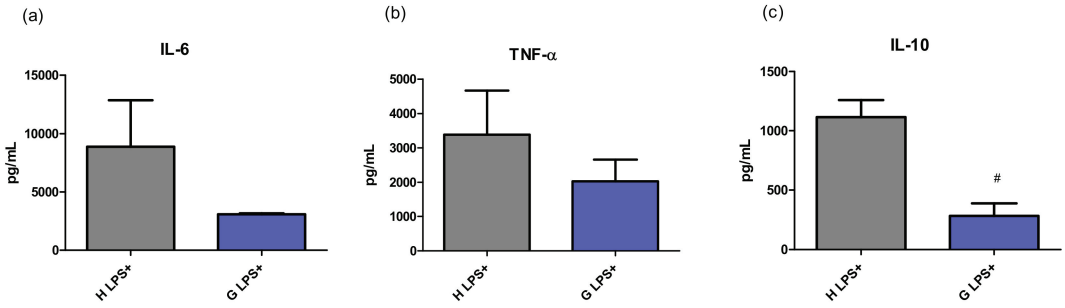

Figure 3. The effect of LPS-induced inflammation on cytokine concentration in serum of hyperbilirubinemic Gunn rats. Concentrations of pro-inflammatory cytokines IL-6, TNF-α, and anti-inflammatory IL-10 were measured 12 h after LPS administration (6 mg/kg i.p.) in normobilirubinemic heterozygous controls (H LPS+) and hyperbilirubinemic Gunn rats (G LPS+), respectively. # $p < 0.05$ vs. LPS-treated group. $n = 5$ animals per group (minimum).

Since the response of an organism to LPS sepsis involves production of LBP, an acute phase protein, by the liver, we tested in whether hyperbilirubinemia might affect production of this mediator. Indeed, *LBP* mRNA expression was upregulated in the liver of Gunn rats compared to in their normobilirubinemic littermates both before (142 ± 37%, $p < 0.05$) and after LPS treatment (148 ± 48%, $p < 0.05$, Figure 4a). Based on the results from in vivo experiments, *LBP* expression in primary hepatocytes was assessed upon exposure to LPS. The expression of *LBP* gradually increased starting at 6 h in Gunn primary hepatocytes exposed to 20 and 40 μM BR ($p < 0.05$, Figure 4b). Interestingly, no significant increase in mRNA expression of *LBP* upon incubation with BR was observed in control hepatocytes (Figure S1, Supplemental Materials).

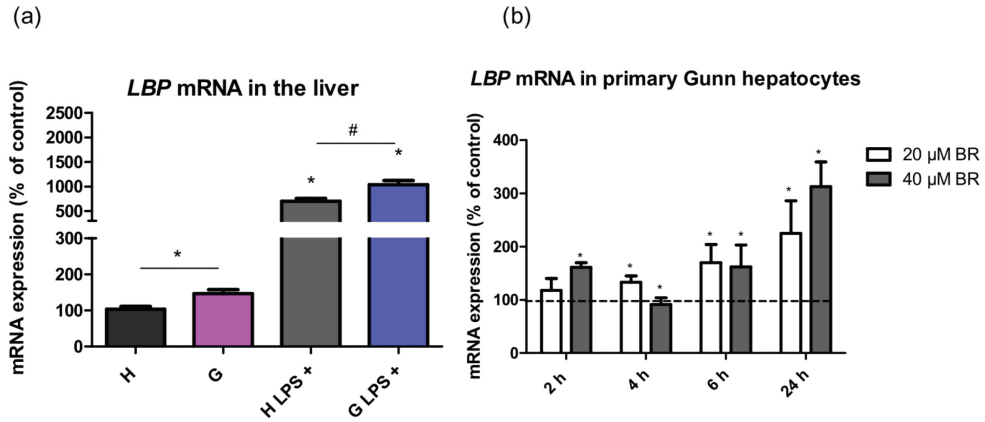

Figure 4. The effects of hyperbilirubinemia on lipopolysaccharide binding protein (*LBP*) mRNA expression in the liver tissues upon exposure to LPS (6 mg/kg i.p.) and in primary hepatocytes. mRNA expression of *LBP* was measured in the liver tissue (**a**) of normobilirubinemic heterozygous controls (H or H LPS+) and hyperbilirubinemic Gunn rats (G or G LPS+), respectively, and in primary hepatocytes (**b**). Primary hepatocytes isolated from Gunn rats were incubated with BR (20 and 40 μM) for 2, 4, 6, and 24 h. (**b**) Values are expressed as % of untreated control cells (100%). * $p < 0.05$ vs. controls, # $p < 0.05$ vs. LPS-treated group. (**a**) $n = 12$ animals per group (minimum); (**b**) $n = 6$ independent cell cultures per group.

Importantly, markers of liver injury such as alanine transaminase (ALT) and aspartate transaminase (AST) activities were lower in the LPS-treated Gunn rats compared to in LPS-treated controls (1.87 ± 1.14 vs. 5.55 ± 3.32 μkat/L, and 4.28 ± 2.26 vs. 6.22 ± 2.88 μkat/L, respectively, $p < 0.05$ for both comparisons, Figure 5a,b).

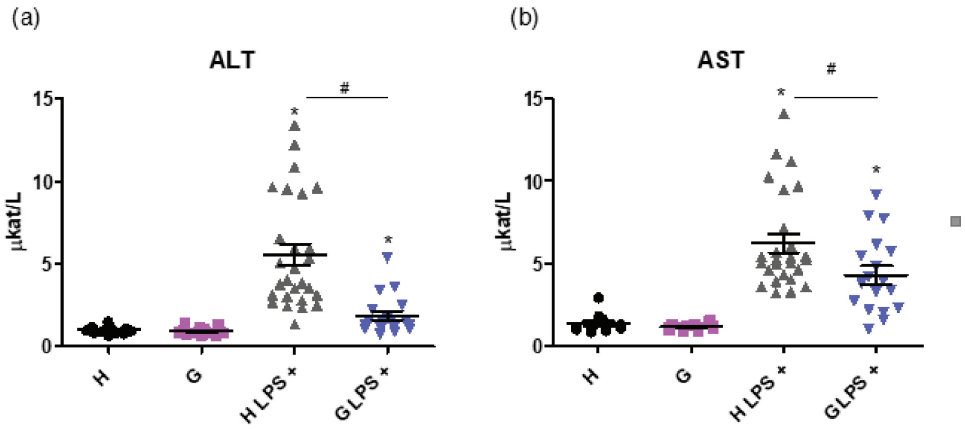

Figure 5. The effect of hyperbilirubinemia and inflammation on markers of the liver injury. ALT (**a**) and AST (**b**) activities, markers of liver injury, were measured in normobilirubinemic heterozygous controls (H or H LPS+) and hyperbilirubinemic Gunn rats (G or G LPS+) 12 h after saline or LPS administration (6 mg/kg i.p.), respectively. * $p < 0.05$ vs. corresponding control, # $p < 0.05$ vs. LPS-treated group. $n = 8$ animals per group (minimum).

2.2. Pretreatment of Primary Hepatocytes with Bilirubin Protects against Inflammation-Induced Cell Death

To assess the underlying mechanisms of anti-inflammatory effect of BR, primary hepatocytes isolated from hyperbilirubinemic Gunn rats and normobilirubinemic heterozygous controls were used for in vitro experiments. Both types of primary liver cells were exposed to BR or/and TNF-α to find out whether constitutive/basal BR could have protective effects on cell viability. No differences in intracellular BR levels were observed between primary hepatocytes isolated from hyperbilirubinemic and normobilirubinemic animals independently of BR treatment (Figure S2a, Supplementary Materials). Nevertheless, primary hepatocytes isolated from hyperbilirubinemic Gunn rats were more resistant to TNF-α-induced cell death as compared to in the control cells (16 ± 10%, $p < 0.05$, Figure S2b), consistent with in vivo data on the effect of hyperbilirubinemia on the liver injury markers described above.

2.3. Effect of Bilirubin on NF-κB Pathway

To examine the role of BR in regulation of NF-κB, a key mediator of inflammatory signaling, we investigated whether BR pre-treatment affects TNF-α-mediated NF-κB activation. Both types of primary hepatocytes were pre-treated with 10–40 μM BR and then exposed to TNF-α. As expected, TNF-α resulted in an increased phosphorylation of the NF-κB p65 subunit. Importantly, pretreatment with BR significantly decreased TNF-α-induced NF-κB p65 subunit phosphorylation (Figure 6a) ($p < 0.05$). No significant changes were detected in total levels of NF-κB p65 protein (Figure 6b), IKKβ protein, and inhibitor IκBα, as well as in phosphorylation of IKKα/β and IκBα after BR and TNF-α treatment (Figure S3). Interestingly, only BR itself increased phosphorylation of IKKα/β (Figure S3).

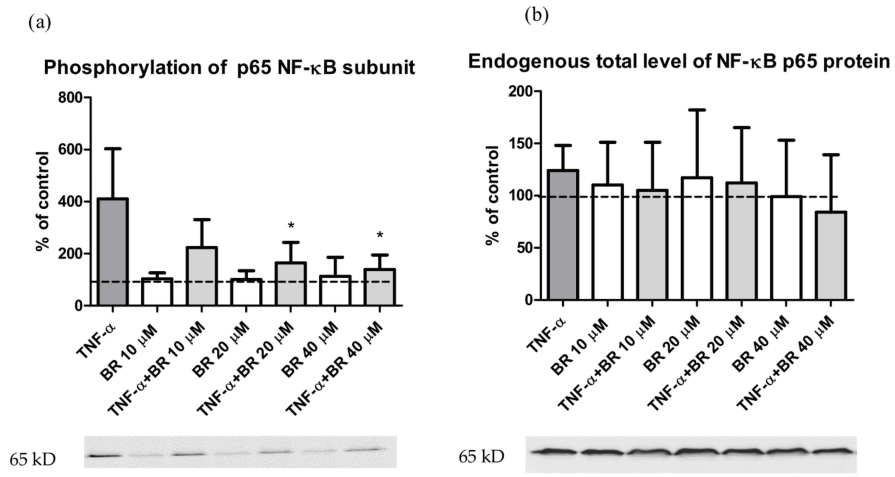

Figure 6. The effect of bilirubin on NF-κB p65 subunit phosphorylation. Both types of primary hepatocytes were pre-incubated with BR (0–40 μM) for 2 h and then treated with TNF-α (12 ng/mL) for 5 min. Phosphorylated (**a**) and total (**b**) NF-κB p65 subunits were measured by the western blot. Values are expressed as % of untreated control cells (100%). * $p < 0.05$ vs. TNF-α. $n = 6$ independent cell cultures per group.

3. Discussion

BR has been shown to be an important cytoprotective and especially antioxidant molecule at physiological or mildly elevated concentrations [1,3]. Even though in vitro studies as well as clinical observations suggest that BR might also possess considerable anti-inflammatory properties [2], surprisingly scarce data have been published on hyperbilirubinemic animal models of inflammation. In our study, we used a model of LPS-induced sepsis in Gunn rats with plasma-unconjugated bilirubin levels at around 60 μmol/L (compared to heterozygotes with 2 μmol/L).

Interestingly, a marked attenuation of WBC pro-inflammatory response with decreased counts of neutrophils and monocytes was observed after LPS treatment in hyperbilirubinemic Gunn animals, accompanied with substantial changes in the $CD4^+/CD8^+$ T cell ratio, an important marker of immune activation [16]. The expansion of $CD8^+$ cells is also driven by the activity of NADPH oxidase (NOX2) [17]. Therefore, the beneficiary $CD4^+/CD8^+$ ratio observed in our study could at least partially be due to a previously reported inhibitory effect of BR on NOX2 activity [18].

The major driving force of neutrophil mobilization from bone marrow and other hematopoetic compartments during sepsis are pro-inflammatory cytokines, of which generation was significantly attenuated in our hyperbilirubinemic rats. Since an overabundance of neutrophils during severe inflammation might have serious damaging effects [19], its amelioration seems to contribute to hyperbilirubinemia-induced protection. In addition, overwhelmed cytokine production during sepsis is also considered detrimental. In fact, lower mortality was observed in rats exposed to LPS and treated with a monoclonal antibody against TNF-α [20], and beneficiary effects were also observed for anti-IL-1β as well as anti-IL-6 antibody treatment in other experimental models of sepsis [21,22].

Together with the decreased expression of pro-inflammatory cytokines observed in our septic hyperbilirubinemic animals, there was also reduced production of IL-10. Although IL-10 is generally considered to be an anti-inflammatory cytokine, its overproduction might also be harmful and result in immunosuppression [23]. In fact, serum IL-10 concentrations were demonstrated in a human clinical study to correlate well with the sepsis severity and mortality, as also did the high IL-10/TNF-α ratio [24]. Thus, the balance between IL-10 and TNF-α seems to be important for immune homeostasis maintenance, as demonstrated by a curative effect of blocking of the IL-10 pathway in several models of bacterial infections such as from *Listeria* [25], *Klebsiella* [26], *Pseudomonas* [23], *Streptococcus* [27], or *Mycobacterium* [28]. It has been suggested that this approach seems to be promising as an adjunct therapy for severe septicemias. In our study, the IL-10/TNF-α ratio was markedly lower

in hyperbilirubinemic Gunn rats, consistent with the better survival rate in Gunn rats exposed to LPS observed in the previous study by Lanone et al. [29]. In concordance with these observations, significantly lower values of hepatocellular liver injury markers were observed in Gunn rats exposed to LPS, as similarly in previous studies [18,29]. In addition, we have previously shown that BR protects the liver against pro-oxidative effects of elevated bile acids in cholestasis [30], further emphasizing the role of BR in hepatoprotection.

To find the factors contributing to a decreased BR-mediated inflammatory response in Gunn rats to LPS, we investigated the expression of LBP in the liver tissue of our experimental animals. LBP, a plasma protein mainly produced by hepatocytes, plays a crucial role in LPS recognition and signaling and is considered an important mediator of the inflammatory reaction [31]. It binds LPS in plasma and transports it via cluster of differentiation 14 (CD14) to the Toll-like receptor 4 (TLR4)/MD-2 signaling complex triggering a range of pro- and anti-inflammatory responses. Dysregulation of this finely tuned signaling cascade could result in a deleterious effect on organism including sepsis and septic shock [32]. Even though the role of LBP in the activation/inhibition of the inflammatory response is probably a dual one, depending on its serum concentration, it has been described that high LBP levels inhibit LPS-mediated cytokine release and prevent hepatic failure in vivo [33]. In our study, hepatic *LBP* expression was significantly higher in Gunn rats before and after LPS treatment, suggesting a role of hyperbilirubinemia in LBP-mediated LPS signaling. Moreover, the treatment of Gunn primary hepatocytes with BR resulted in an increased *LBP* expression, indicating that BR might affect LBP production, and thus contribute to an attenuated inflammatory response in hyperbilirubinemic subjects.

The production of pro-inflammatory cytokines during sepsis leads to activation of NF-κB [34]. In fact, our experiments on primary rat hepatocytes demonstrated that BR exposure resulted in decreased phosphorylation of the p65 subunit of the NF-κB protein complex, a phenomenon which might be related to both general inhibitory effects of BR on protein phosphorylation [15], as well as inhibition of phosphorylation via suppressed TNF-α signaling [35]. It is thus likely that anti-inflammatory and cytoprotective effects of BR may at least in part be due to attenuation of NF-κB-driven transcription. On the contrary, we did not observe any inhibition of IκB phosphorylation, which has previously been reported, but at much higher BR levels [10]. Moreover, phosphorylation of IKK was increased by BR itself. Our data are consistent with previous reports demonstrating this specific inhibitory effect of both BR [36] and biliverdin [37,38]. It is also interesting to note that the $CD4^+/CD8^+$ ratio (similarly to Tregs and myelopoesis), which changes in our hyperbilirubinemic rats, is also regulated by the activity of NF-κB [39].

Furthermore, Gunn rat hepatocytes were more resistant to TNF-α-induced cytotoxicity, although no changes in intracellular BR concentrations were observed compared to control cells. These data suggest that not only BR itself, but also "bilirubin priming", triggering adaptive, para-hormetic mechanisms under hyperbilirubinemic conditions, might significantly contribute to the observed hepatoprotection; however, intensive research is needed to identify these mechanisms.

4. Materials and Methods

4.1. Chemicals and Reagents

BR, the bovine serum albumin (BSA), rat TNF-α, LPS from Escherichia coli 0114:B4, human insulin solution, Williams' E Medium, Collagen type I from rat tail tendon, 2,6-di-tert-butyl-4-methylphenol (BHT), Thiazolyl Blue Tetrazolium Bromide (MTT), RNAlater, and tetrabutyl-ammonium hydroxide (TBA, 40 % in water) were purchased from Sigma-Aldrich (St. Louis, MO, USA); the chloroform (HPLC grade), methanol (HPLC grade), *n*-hexane, ethyl acetate, and acetonitrile were purchased from Merck (Darmstadt, Germany); and 4×-Laemmli sample buffer was from Bio-Rad (Hercules, CA, USA).

As described earlier, the BR was purified before use [40]. For the experiments, BR (2.8 mg) was dissolved in 2 mL of 0.1 M NaOH and immediately mixed with 1 mL of 0.1 M phosphoric acid. The mixture was diluted with a BSA solution (660 μM BSA in 25 mM phosphate buffer, pH: 7.7) to

reach a final concentration of 480 μM BR in a phosphate buffer and then serially diluted with a BSA solution to yield solutions with final BR concentrations within the range of 10–40 μM.

4.2. In Vivo Studies

Hyperbilirubinemic adult female Gunn rats and their normobilirubinemic heterozygous littermates (*n* range: 8–25 per group, weight range: 160–260 g) had access to water and food ad libitum. Gunn rats were kindly provided by Cluster in Biomolecular Medicine (University of Trieste, Italy). All protocols were approved by the Animal Research Committee of the 1st Faculty of Medicine, Charles University, project No. MSMT-25538/2018-2 (29 August 2018) as well as by the Institute of Molecular Genetics of the Academy of the Sciences of the Czech Republic, project No. PP 67/2018 (24 July 2018) and carried out in accordance with the Guide for the Care and Use of Animals of the National Institutes of Health.

The rats were divided into 4 groups: normobilirubinemic heterozygote (a) and hyperbilirubinemic Gunn (b) experimental groups were treated with LPS (H LPS+/G LPS+, 6 mg/kg intraperitoneally); and normobilirubinemic heterozygote (c) and hyperbilirubinemic Gunn (d) control groups received vehicle (saline). After 12 h, the animals were anesthetized (xylazin: 16 mg/kg, i.m.) and sacrificed. Blood for further biochemical analyses was obtained from the inferior vena cava and from the aorta for flow cytometry. Relevant organs (liver, heart, lung, kidney, spleen, and brain) were harvested, washed with ice-cold PBS, snap frozen in liquid nitrogen and stored at −80 °C. For RNA analysis, 100 mg of fresh liver was immediately placed in 2-mL microfuge tubes containing RNAlater and stored according to the manufacturer's instructions until analysis.

4.3. Determination of Complete Blood Count with Differential and Serum Biochemical Markers

Complete blood counts were measured from whole blood using an XN-1000™ automatic analyzer (Sysmex, Lincolnshire, IL, USA). Serum biochemical markers (ALT and AST activities) were determined by standard assays using an automatic analyzer (Modular analyzer, Roche Diagnostics GmbH, Mannheim, Germany).

4.4. Determination of Serum Cytokine Concentrations

Determination of serum cytokine concentrations were performed using commercial rat ELISA kits (Duo-Sets kits for IL-1β/IL-1F2, IL-10, TNF-α, and IL-6; Bio-Techne R&D Systems, Minneapolis, MN, USA) according to the manufacturer's instructions.

4.5. Flow Cytometry of Lymphocytes

Blood samples (250 μL of whole blood) were collected in tubes with 3% potassium EDTA. After lysis of the red blood cells (twice) using ACK buffer (0.15 M NH4Cl, 10 mM KHCO3, and 1 mM EDTA monosodium; pH: 7.3) for 15 and 5 min separately, followed by washing with PBS (twice), the cells were simultaneously stained for effector T cells. Cells were surface-stained using the following anti-rat antibodies: anti-CD45-FITC (OX-1, Thermo Fisher Scientific, Waltham, MA, USA), anti-CD4-BV-786 (OX-35, BD Biosciences, San Jose, CA, USA), anti-CD8α-PerCP-e710 (OX-8, Thermo Fisher Scientific), and anti-CD62L-PE (OX-85, SONY) for CD4/CD8 T cells panel. The cell suspensions were analyzed by flow cytometry (BD LSR II including an FACSFlow Supply of the High Throughput Sampler System, BD Biosciences).

4.6. Gene Expression Analyses

Total RNA from liver tissue and blood was isolated using a GenUP™ Total RNA Kit (Biotechrabbit GmbH, Hennigsdorf, Germany) and a Total RNA Mini Kit (Geneaid Biotech Ltd, New Taipei City, Taiwan), respectively. The quantity and purity of isolated RNA were evaluated spectrophotometrically. cDNA was generated by a High-Capacity cDNA Reverse Transcription Kit (Thermo Fisher Scientific) and stored at −20 °C until analysis. Quantitative real-time PCR was performed using TaqMan® Fast Advanced Master Mix and a TaqMan® Gene Expression Assay Kit for the following genes: *IL-6*

(Rn01410330_m1), *TNF-α* (Rn99999017_m1), *IL-10* (Rn00563409_m1), *IL-1β* (Rn00580432_m1), *LBP* (Rn00567985_m1), and a rat endogenous control β-2 microglobulin (Rn005608865_m1). Results were expressed as the % of controls.

4.7. Primary Rat Hepatocyte Culture

Primary hepatocytes were isolated from anaesthetized Gunn and heterozygote (n = 3 each, weight range: 200–220 g) rats by two-step collagenase perfusion according to a published protocol [41]. Cell viability ranged from 75% to 85% (as trypan blue staining). Hepatocytes were further diluted to 0.8 million cells/mL with William's E medium, supplemented with 1% penicillin/streptomycin, 1% L-glutamine, 0.06% insulin, and 5% fetal bovine serum. Primary hepatocytes were dispensed into a collagen-coated cell culture Petri dishes, 6-well and 96-well plates and allowed to attach for 3 h at 37 °C with 5% CO_2 in the incubator. Unattached cells were removed after 3 h and a new medium was added. The following day, hepatocytes were cultured with complete culture medium containing BR (10–40 μM) and TNF-α (12–100 ng/mL) for 24 h.

4.8. Determination of Cell Viability and Intracellular Bilirubin Levels

All experiments were performed under dim light to minimize BR degradation. Cell viability of primary hepatocytes seeded in 96-well plates was measured using an MTT test after 24 h incubation. Primary hepatocytes harvested from 10 cm Petri dishes were used for determination of intracellular BR as described previously [42].

4.9. Western Blot Analysis

Primary hepatocytes were lysed using a lysis buffer (5 M NaCl, 1 M Tris, pH = 8, 10% Triton-X 100), sonicated for 5 s and centrifuged at a speed of 14,000× g for 10 min (temperature: 4 °C). Supernatants (35–40 μg of protein) were diluted with a loading buffer (4× Laemmli Sample buffer, Bio-Rad, USA), denatured at 95 °C for 10 min, and separated by SDS-PAGE electrophoresis (10%). Proteins were transferred to a nitrocellulose membrane, blocked in 5% BSA in TTBS for 1.5 h and then incubated overnight at 4 °C with primary antibodies anti phospho-NF-κB p65 (Ser536) (dilution, 1:2000 v/v), anti NF-κB p65 (dilution, 1:3500 v/v), anti IκB-α (dilution, 1:3500 v/v), anti phospo-IκB-α (Ser132) (dilution, 1:1500 v/v), anti IKKβ (dilution, 1:3500 v/v), anti phospho-IKKα/β (Ser176/180) (dilution, 1:1500 v/v), as well as anti β-actin (dilution, 1:5000 v/v) as a loading control (all antibodies were from Cell Signaling Technology, Danvers, MA, USA). After being washed in TTBS buffer, membranes were incubated with swine anti-rabbit IgG-HRP secondary antibody (Dako, Glostrup, Denmark) and visualized using an ECL kit (LumiGLO®, Cell Signaling Technology). A Fusion Fx7 device and Bio-2D software (Vilber Lourmat, Collegien, France) were used to quantify the signals. Results were normalized to β-actin.

4.10. Statistical Analysis

Student parametric unpaired and paired t-tests were used for comparison of normally distributed data. Non-normally distributed data were analyzed with the Mann–Whitney rank sum test. Group mean differences were analyzed by ANOVA and Kruskal–Wallis tests. Depending on their normality, data are expressed as the mean with SD or the median with interquartile range. Differences were considered statistically significant when $p < 0.05$. Analyses were performed using GraphPad Prism 5.0 statistical software (GraphPad Software, Inc., San Diego, CA, USA).

5. Conclusions

In conclusion, hyperbilirubinemia in Gunn rats is associated with an attenuated systemic inflammatory response and decreased liver damage upon exposure to LPS, an effect associated with a modulation of innate immunity together with decreased production of pro-inflammatory cytokines and NF-κB activation.

Supplementary Materials: Supplementary materials can be found at http://www.mdpi.com/1422-0067/20/9/2306/s1. Figure S1: The effects of BR on LBP mRNA expression in primary heterozygote hepatocytes; Figure S2: The effects of BR and TNF-α on viability of primary hepatocytes; Figure S3: The effect of bilirubin on the NF-κB signaling pathway.

Author Contributions: Conceptualization, L.M. and L.V.; data curation, P.V.; formal analysis, P.V. and M.L.; funding acquisition, L.V.; methodology, P.V., L.M., K.Z., and L.V.; project administration, P.V., A.D., and K.Z.; supervision, L.V.; writing of an original draft, P.V.; writing of review and editing, L.M., M.L., A.D., J.Z., M.C., N.K.C. and L.V. All authors participated in reviewing the manuscript.

Funding: This research was funded by grants GAUK 168216 given by the First Faculty of Medicine, Charles University, Prague, Czech Republic, SVV 260370/2018 given by Charles University, Prague, Czech Republic, and RVO-VFN64165/2018 given by the Czech Ministry of Health.

Acknowledgments: We wish to thank Marie Zadinova, Libuse Slehobrova, Karel Chalupsky, and Peter Neradil for their excellent technical assistance during the animal studies.

Conflicts of Interest: The authors declare no conflicts of interest.

Abbreviations

ALT	Alanine transaminase
AST	Aspartate transaminase
BR	Bilirubin
IKK	IκB kinase
IL-6	Interleukin-6
IL-10	Interleukin-10
IL-1β	Interleukin-1β
LBP	Lipopolysaccharide-binding protein
LPS	Lipopolysaccharide
NF-κB	Nuclear factor kappa B
TLR	Toll-like receptors
TNF-α	Tumor necrosis factor-α
TLR	Toll-like receptor
WBC	White blood cell

References

1. Gazzin, S.; Vitek, L.; Watchko, J.; Shapiro, S.M.; Tiribelli, C. A novel perspective on the biology of bilirubin in health and disease. *Trends Mol. Med.* **2016**, *22*, 758–768. [CrossRef] [PubMed]
2. Jangi, S.; Otterbein, L.; Robson, S. The molecular basis for the immunomodulatory activities of unconjugated bilirubin. *Int. J. Biochem. Cell B* **2013**, *45*, 2843–2851. [CrossRef] [PubMed]
3. Wagner, K.H.; Wallner, M.; Molzer, C.; Gazzin, S.; Bulmer, A.C.; Tiribelli, C.; Vitek, L. Looking to the horizon: The role of bilirubin in the development and prevention of age-related chronic diseases. *Clin. Sci.* **2015**, *129*, 1–25. [CrossRef]
4. Basiglio, C.L.; Arriaga, S.M.; Pelusa, F.; Almara, A.M.; Kapitulnik, J.; Mottino, A.D. Complement activation and disease: Protective effects of hyperbilirubinaemia. *Clin. Sci.* **2010**, *118*, 99–113. [CrossRef] [PubMed]
5. Adin, C.A.; VanGundy, Z.C.; Papenfuss, T.L.; Xu, F.; Ghanem, M.; Lakey, J.; Hadley, G.A. Physiologic doses of bilirubin contribute to tolerance of islet transplants by suppressing the innate immune response. *Cell Transplant.* **2017**, *26*, 11–21. [CrossRef]
6. Idelman, G.; Smith, D.L.H.; Zucker, S.D. Bilirubin inhibits the up-regulation of inducible nitric oxide synthase by scavenging reactive oxygen species generated by the toll-like receptor 4-dependent activation of NADPH oxidase. *Redox Biol.* **2015**, *5*, 398–408. [CrossRef]
7. Vetvicka, V.; Miler, I.; Sima, P.; Taborsky, L.; Fornusek, L. The effect of bilirubin on the Fc receptor expression and phagocytic activity of mouse peritoneal macrophages. *Folia Microbiol.* **1985**, *30*, 373–380. [CrossRef]
8. Nejedla, Z. The development of immunological factors in infants with hyperbilirubinemia. *Pediatrics* **1970**, *45*, 102–104.
9. Rocuts, F.; Zhang, X.Y.; Yan, J.; Yue, Y.A.; Thomas, M.; Bach, F.H.; Czismadia, E.; Wang, H.J. Bilirubin promotes de novo generation of T regulatory cells. *Cell Transplant.* **2010**, *19*, 443–451. [CrossRef]

10. Liu, Y.; Li, P.; Lu, J.; Xiong, W.; Oger, J.; Tetzlaff, W.; Cynader, M. Bilirubin possesses powerful immunomodulatory activity and suppresses experimental autoimmune encephalomyelitis. *J. Immunol.* **2008**, *181*, 1887–1897. [CrossRef]
11. Haga, Y.; Tempero, M.A.; Kay, D.; Zetterman, R.K. Intracellular accumulation of unconjugated bilirubin inhibits phytohemagglutin-induced proliferation and interleukin-2 production of human lymphocytes. *Dig. Dis. Sci.* **1996**, *41*, 1468–1474. [CrossRef]
12. Lawrence, T. The nuclear factor NF-kappaB pathway in inflammation. *Cold Spring Harb. Perspect. Biol.* **2009**, *1*, a001651. [CrossRef]
13. Jerala, R. Structural biology of the LPS recognition. *Int. J. Med. Microbiol.* **2007**, *297*, 353–363. [CrossRef]
14. Siebenlist, U.; Franzoso, G.; Brown, K. Structure, regulation and function of Nf-Kappa-B. *Annu. Rev. Cell Biol.* **1994**, *10*, 405–455. [CrossRef]
15. Hansen, T.W.R.; Mathiesen, S.B.W.; Walaas, S.I. Bilirubin has widespread inhibitory effects on protein phosphorylation. *Pediatr. Res.* **1996**, *39*, 1072–1077. [CrossRef]
16. Bruno, G.; Saracino, A.; Monno, L.; Angarano, G. The Revival of an "Old" Marker: CD4/CD8 Ratio. *Aids Rev.* **2017**, *19*, 81–88.
17. Dhiman, M.; Garg, N.J. P47(phox-/-)mice are compromised in expansion and activation of CD8(+) T cells and susceptible to trypanosoma cruzi infection. *PLoS Pathog.* **2014**, *10*, e1004516. [CrossRef]
18. Wang, W.Z.W.; Smith, D.L.H.; Zucker, S.D. Bilirubin inhibits iNOS expression and NO production in response to endotoxin in rats. *Hepatology* **2004**, *40*, 424–433. [CrossRef] [PubMed]
19. Summers, C.; Rankin, S.M.; Condliffe, A.M.; Singh, N.; Peters, A.M.; Chilvers, E.R. Neutrophil kinetics in health and disease. *Trends Immunol.* **2010**, *31*, 318–324. [CrossRef]
20. Ozer, E.K.; Goktas, M.T.; Kilinc, I.; Toker, A.; Bariskaner, H.; Ugurluoglu, C.; Iskit, A.B. Infliximab alleviates the mortality, mesenteric hypoperfusion, aortic dysfunction, and multiple organ damage in septic rats. *Can. J. Physiol. Pharm.* **2017**, *95*, 866–872. [CrossRef] [PubMed]
21. Ohlsson, K.; Bjork, P.; Bergenfeldt, M.; Hageman, R.; Thompson, R.C. Interleukin-1 receptor antagonist reduces mortality from endotoxin-shock. *Nature* **1990**, *348*, 550–552. [CrossRef]
22. Nullens, S.; Staessens, M.; Peleman, C.; Plaeke, P.; Malhotra-Kumar, S.; Francque, S.; De Man, J.G.; De Winter, B.Y. Beneficial effects of anti-interleukin-6 antibodies on impaired gastrointestinal motility, inflammation and increased colonic permeability in a murine model of sepsis are most pronounced when administered in a preventive setup. *PLoS ONE* **2016**, *11*, e0152914. [CrossRef] [PubMed]
23. Steinhauser, M.E.; Hogaboam, G.M.; Kunkel, S.L.; Lukacs, N.W.; Strieter, R.M.; Standiford, T.J. IL-10 is a major mediator of sepsis-induced impairment in lung antibacterial host defense. *J. Immunol.* **1999**, *162*, 392–399.
24. Gogos, C.A.; Drosou, E.; Bassaris, H.P.; Skoutelis, A. Pro- versus anti-inflammatory cytokine profile in patients with severe sepsis: A marker for prognosis and future therapeutic options. *J. Infect. Dis.* **2000**, *181*, 176–180. [CrossRef]
25. Silva, R.A.; Appelberg, R. Blocking the receptor for interleukin 10 protects mice from lethal listeriosis. *Antimicrob. Agents Chempther.* **2001**, *45*, 1312–1314. [CrossRef]
26. Wang, M.J.; Jeng, K.C.G.; Ping, L.I. Exogenous cytokine modulation or neutralization of interleukin-10 enhance survival in lipopolysaccharide-hyporesponsive C3H/HeJ mice with Klebsiella infection. *Immunology* **1999**, *98*, 90–97. [CrossRef] [PubMed]
27. Van der Poll, T.; Marchant, A.; Keogh, C.B.; Goldman, M.; Lowry, S.F. Interleukin-10 impairs host defense in murine pneumococcal pneumonia. *J. Infect. Dis.* **1996**, *174*, 994–1000. [CrossRef]
28. Jacobs, M.; Brown, N.; Allie, N.; Gulert, R.; Ryffel, B. Increased resistance to mycobacterial infection in the absence of interleukin-10. *Immunology* **2000**, *100*, 494–501. [CrossRef] [PubMed]
29. Lanone, S.; Bloc, S.; Foresti, R.; Almolki, A.; Taille, C.; Callebert, J.; Conti, M.; Goven, D.; Aubier, M.; Dureuil, B.; et al. Bilirubin decreases nos2 expression via inhibition of NAD(P)H oxidase: Implications for protection against endotoxic shock in rats. *FASEB J.* **2005**, *19*, 1890–1892. [CrossRef]
30. Muchova, L.; Vanova, K.; Zelenka, J.; Lenicek, M.; Petr, T.; Vejrazka, M.; Sticova, E.; Vreman, H.J.; Wong, R.J.; Vitek, L. Bile acids decrease intracellular bilirubin levels in the cholestatic liver: Implications for bile acid-mediated oxidative stress. *J. Cell Mol. Med.* **2011**, *15*, 1156–1165. [CrossRef]

31. Su, G.L.; Freeswick, P.D.; Geller, D.A.; Wang, Q.; Shapiro, R.A.; Wan, Y.H.; Billiar, T.R.; Tweardy, D.J.; Simmons, R.L.; Wang, S.C. Molecular-cloning, characterization, and tissue distribution of rat lipopolysaccharide-binding protein - evidence for extrahepatic expression. *J. Immunol.* **1994**, *153*, 743–752.
32. Shimazu, R.; Akashi, S.; Ogata, H.; Nagai, Y.; Fukudome, K.; Miyake, K.; Kimoto, M. MD-2, a molecule that confers lipopolysaccharide responsiveness on Toll-like receptor 4. *J. Exp. Med.* **1999**, *189*, 1777–1789. [CrossRef]
33. Lamping, N.; Dettmer, R.; Schroder, N.W.J.; Pfeil, D.; Hallatschek, W.; Burger, R.; Schumann, R.R. LPS-binding protein protects mice from septic shock caused by LPS or gram-negative bacteria. *J. Clin. Investig.* **1998**, *101*, 2065–2071. [CrossRef] [PubMed]
34. Perkins, N.D. Integrating cell-signalling pathways with NF-kappa B and IKK function. *Nat. Rev. Mol. Cell. Bio.* **2007**, *8*, 49–62. [CrossRef]
35. Mazzone, G.L.; Rigato, I.; Ostrow, J.D.; Tiribelli, C. Bilirubin effect on endothelial adhesion molecules expression is mediated by the NF-kappa B signaling pathway. *Biosci. Trends* **2009**, *3*, 151–157. [PubMed]
36. Soares, M.P.; Seldon, M.P.; Gregoire, I.P.; Vassilevskaia, T.; Berberat, P.O.; Yu, J.; Tsui, T.Y.; Bach, F.H. Heme oxygenase-1 modulates the expression of adhesion molecules associated with endothelial cell activation. *J. Immunol.* **2004**, *172*, 3553–3563. [CrossRef]
37. Gibbs, P.E.M.; Maines, M.D. Biliverdin inhibits activation of NF-kappa B: Reversal of inhibition by human biliverdin reductase. *Int. J. Cancer* **2007**, *121*, 2567–2574. [CrossRef]
38. Nuhn, P.; Mitkus, T.; Ceyhan, G.O.; Kunzli, B.M.; Bergmann, F.; Fischer, L.; Giese, N.; Friess, H.; Berberat, P.O. Heme oxygenase 1-generated carbon monoxide and biliverdin attenuate the course of experimental necrotizing pancreatitis. *Pancreas* **2013**, *42*, 265–271. [CrossRef] [PubMed]
39. Jimi, E.; Strickland, I.; Voll, R.E.; Long, M.X.; Ghosh, S. Differential role of the transcription factor NF-kappa B in selection and survival of CD4(+) and CD8(+) thymocytes. *Immunity* **2008**, *29*, 523–537. [CrossRef]
40. McDonagh, A.F.; Assisi, F. The ready isomerization of bilirubin IX- in aqueous solution. *Biochem. J.* **1972**, *129*, 797–800. [CrossRef]
41. Berry, M.N.; Grivell, A.R.; Grivell, M.B.; Phillips, J.W. Isolated hepatocytes-past, present and future. *Cell Biol. Toxicol.* **1997**, *13*, 223–233. [CrossRef] [PubMed]
42. Zelenka, J.; Lenicek, M.; Muchova, L.; Jirsa, M.; Kudla, M.; Balaz, P.; Zadinova, M.; Ostrow, J.D.; Wong, R.J.; Vitek, L. Highly sensitive method for quantitative determination of bilirubin in biological fluids and tissues. *J. Chromatogr. B* **2008**, *867*, 37–42. [CrossRef] [PubMed]

Hindawi
Oxidative Medicine and Cellular Longevity
Volume 2018, Article ID 3845027, 12 pages
https://doi.org/10.1155/2018/3845027

Research Article

Heme Oxygenase-1 May Affect Cell Signalling via Modulation of Ganglioside Composition

Václav Šmíd,[1,2] **Jakub Šuk**,[1] **Neli Kachamakova-Trojanowska**,[3,4] **Jana Jašprová**,[1] **Petra Valášková**,[1] **Alicja Józkowicz**,[3] **Józef Dulak**,[3] **František Šmíd**,[1] **Libor Vítek**,[1,2] **and Lucie Muchová**[1]

[1]*Institute of Medical Biochemistry and Laboratory Diagnostics, 1st Faculty of Medicine and General University Hospital in Prague, Charles University, Katerinska 32, 12108 Prague, Czech Republic*
[2]*4th Department of Internal Medicine, 1st Faculty of Medicine and General University Hospital in Prague, Charles University, U Nemocnice 499/2, 12801 Prague, Czech Republic*
[3]*Department of Medical Biotechnology, Faculty of Biochemistry, Biophysics and Biotechnology, Jagiellonian University, 7 Gronostajowa St., 30-387 Krakow, Poland*
[4]*Malopolska Centre for Biotechnology, Jagiellonian University, Gronostajowa str 7a, 30-387 Krakow, Poland*

Correspondence should be addressed to Lucie Muchová; lucie.muchova@lf1.cuni.cz

Received 14 May 2018; Revised 28 July 2018; Accepted 5 August 2018; Published 19 September 2018

Academic Editor: Daniele Vergara

Heme oxygenase 1 (Hmox1), a ubiquitous enzyme degrading heme to carbon monoxide, iron, and biliverdin, is one of the cytoprotective enzymes induced in response to a variety of stimuli, including cellular oxidative stress. Gangliosides, sialic acid-containing glycosphingolipids expressed in all cells, are involved in cell recognition, signalling, and membrane stabilization. Their expression is often altered under many pathological and physiological conditions including cell death, proliferation, and differentiation. The aim of this study was to assess the possible role of Hmox1 in ganglioside metabolism in relation to oxidative stress. The content of liver and brain gangliosides, their cellular distribution, and mRNA as well as protein expression of key glycosyltransferases were determined in *Hmox1* knockout mice as well as their wild-type littermates. To elucidate the possible underlying mechanisms between Hmox1 and ganglioside metabolism, hepatoblastoma HepG2 and neuroblastoma SH-SY5Y cell lines were used for *in vitro* experiments. Mice lacking *Hmox1* exhibited a significant increase in concentrations of liver and brain gangliosides and in mRNA expression of the key enzymes of ganglioside metabolism. A marked shift of GM1 ganglioside from the subsinusoidal part of the intracellular compartment into sinusoidal membranes of hepatocytes was shown in *Hmox1* knockout mice. Induction of oxidative stress by chenodeoxycholic acid *in vitro* resulted in a significant increase in GM3, GM2, and GD1a gangliosides in SH-SY5Y cells and GM3 and GM2 in the HepG2 cell line. These changes were abolished with administration of bilirubin, a potent antioxidant agent. These observations were closely related to oxidative stress-mediated changes in sialyltransferase expression regulated at least partially through the protein kinase C pathway. We conclude that oxidative stress is an important factor modulating synthesis and distribution of gangliosides *in vivo* and *in vitro* which might affect ganglioside signalling in higher organisms.

1. Introduction

Heme oxygenase 1 (Hmox1) is a highly inducible antioxidant and cytoprotective enzyme in the heme catabolic pathway generating equimolar amounts of iron, carbon monoxide, and biliverdin which is immediately reduced to bilirubin [1]. Hmox1 activity—also due to the effect of its bioactive products—affects pathophysiology of many neurologic, cardiovascular, and pulmonary diseases [2–4]. In the liver, Hmox1 plays an important role in hepatic fat accumulation, fibrogenesis, ischemia-reperfusion, and oxidative injury [5]. Moreover, upon *Hmox1* knockout, the cells and/or animals become more vulnerable to oxidative stress. Free radical formation as well as oxidative stress-

associated cytotoxicity are increased in *Hmox1* knockouts due to reduced antioxidant bilirubin and vasoactive carbon monoxide formation, disruption of iron homeostasis, and accumulation of prooxidative heme [6]. Due to iron accumulation, liver is one of the tissues most affected by an increased oxidative stress in *Hmox1* knockout mice and increased lipid peroxidation, fibrosis, and hepatic injury have been described in these animals [5]. Furthermore, an increase in some key cytoprotective genes such as NAD(P)H dehydrogenase quinone 1 and glutathione S-transferase P1 and marked decrease in peroxyl radical scavenging activity have been described in *Hmox1* knockouts even under basal (unstimulated) conditions [7]. Bilirubin per se is considered a potent endogenous antioxidant protecting against diseases associated with oxidative stress [8] and counteracting harmful effects of various prooxidants including hydrophobic bile acids (BA) on cells and tissues [9]. In fact, both bilirubin and BA are accumulated in plasma and tissues during cholestasis and while BA are responsible for increased lipid peroxidation and oxidative liver damage, bilirubin has a protective effect [10].

Gangliosides are ubiquitously found in all tissues, but most abundantly in the nervous system [11]. They substantially influence the organization of the membrane and the function of specific membrane-associated proteins due to lipid-lipid and lipid-protein lateral interactions [12]. In the brain, ganglioside expression correlates with neurogenesis, synaptogenesis, synaptic transmission, and cell proliferation [13, 14].

It is known that gangliosides form so called caveolae or "detergent resistant microdomains" (DRM), which are crucial elements for cell-cell recognition, adhesion, and especially membrane stabilization [15, 16]. There is also evidence that caveolin-1, an important component of caveolae, interacts with Hmox1, modulates its activity, and can act as a natural competitive inhibitor of Hmox1 with heme [17]. Moreover, gangliosides have been found to inhibit hydroxyl radical formation *in vitro* [18] and also modulate ROS formation in human leukocytes [19] and neuronal cells [20].

Despite the close relationship of gangliosides and Hmox1 in DRM, there are only few reports discussing the possible role of Hmox1 or oxidative stress in ganglioside metabolism [21, 22]. The aim of this study was to assess the role of *Hmox1* knockout and associated oxidative stress on ganglioside metabolism and to identify the possible underlying mechanisms.

2. Materials and Methods

2.1. Materials. Paraformaldehyde, biotin, bovine serum albumin (BSA), phorbol 12-myristate 13-acetate (protein kinase C (PKC) activator), Ro 31-0432 (PKC inhibitor), chenodeoxycholic acid (CDCA), diaminobenzidine tetrahydrochloride tablets, NADPH, and sulfosalicylic acid were supplied by Sigma-Aldrich (St. Louis, MO, USA); avidin was obtained from Fluka (Buchs, Switzerland), the cholera toxin B subunit (CTB) peroxidase conjugated came from List Biological Laboratories (CA, USA), and the HPTLC silica-gel plates came from Merck (Darmstadt, Germany). Cell plates were supplied by Corning (NY, USA). The TaqMan® Gene Expression Master Mix, High-Capacity RNA-to-cDNA Kit, and the TaqMan Gene Expression Assay kit for mouse and human genes were obtained from Life Technologies (Carlsbad, CA, USA). The QIAshredder kit and RNeasy Plus Mini Kit were supplied by Qiagen (USA). All other chemicals were purchased locally from Penta (Prague, Czech Republic).

2.2. Animals. $Hmox1^{-/-}$ ($n = 9$; KO—knockout) mice and $Hmox1^{+/+}$ ($n = 6$; Wt—wild type) littermates (C57Bl/6xFVB, 8-week-old males) were used for all the experiments. Breeding heterozygote pairs of *Hmox1*-deficient mice were initially kindly provided by Anupam Agarwal, University of Alabama (Birmingham, AL). The $Hmox1^{-/-}$ strain poorly breeds on pure C57/Bl6 background (5.1% of expected $Hmox1^{-/-}$ pups) and therefore is maintained on mixed C57/Bl6 × FVB background (20.1% of expected $Hmox^{-/-}$ pups, when $Hmox^{-/-}$ males are crossed with $Hmox^{+/-}$ females) [23]. All $Hmox1^{+/+}$ controls were C57/Bl6xFVB littermates from the same breeders used to obtain $Hmox1^{-/-}$ mice. They had free access to food and water and were kept in individually ventilated cages with a 12:12 day/night cycle, under a specific pathogen-free regime. All aspects of the study met the accepted criteria of experimental use of laboratory animals, and all protocols were approved by the Animal Research Committee of the 1st Faculty of Medicine, Charles University, Prague, Czech Republic, and by the 1st Local Ethics Committee for Animal Research, Krakow, Poland.

2.3. Tissue Preparation. Mice were intraperitoneally anesthetized with ketamine (90 mg/kg) and xylazine (10 mg/kg) and sacrificed by cervical dislocation at day 5. The inferior vena cava was cannulated through laparotomy, and blood samples were collected, transferred to EDTA-containing tubes, mixed, and placed on ice. An aliquot was centrifuged to separate out the plasma. The livers and brains were then harvested and weighed. Pieces of liver tissues were appropriately processed for further biochemical and histochemical analyses (see below). For quantitative histochemical analysis of GM1 ganglioside, the liver specimens were collected using a systematic uniform random sampling method [24].

For the RNA analysis, 100 mg of tissue was immediately placed in 1.5 mL microcentrifuge tubes containing RNAlater (Qiagen, Valencia, CA, USA). The tubes were stored at −80°C until total RNA isolation.

2.4. Extraction and TLC Densitometry of Liver and Brain Gangliosides. The chloroform-methanol extraction of gangliosides from the liver tissue was used—the procedure previously described by Majer et al. [25]—and gangliosides were finally purified on a small silica gel column [26]. Brain gangliosides were isolated as described previously [27, 28]. All ganglioside samples were separated in a solvent system (chloroform/methanol/0.2% aqueous $CaCl_2$, 55/45/10, *v*/*v*/*v*) and detected with resorcinol-HCl reagent. The densitometry was performed according to Majer et al. [25] using a CATS3 Software, CAMAG (Switzerland).

GSL are abbreviated according to recommendations of the IUPAC-IUB Commission on Biochemical Nomenclature [29]: glycosyltransferases: *GlcT*, UDP-glucose ceramide

glucosyltransferase; *GalTI*, UDP-Gal:betaGlcNAc beta-1,4-galactosyltransferase; *ST3GalV (GM3 synthase)*, ST3 beta-galactoside alpha-2,3-sialyltransferase 5; *ST8SiaI (GD3 synthase)*, ST8 alpha-*N*-acetylneuraminide alpha-2,8-sialyltransferase 1; *B4GalNTI (GM2/GD2 synthase)*, beta-1,4-*N*-acetyl-galactosaminyltransferase 1; and *B3GalTIV (GM1 synthase)*, UDP-Gal:betaGlcNAc beta 1,3-galactosyltransferase.

2.5. GM1 Histochemistry. GM1 was determined using a modified procedure according to Jirkovská et al. [30]. In brief, 4% formaldehyde was freshly prepared by depolymerization of paraformaldehyde (pH = 7.2). Frozen 6 μm thin sections were first fixed in dry cold acetone (−20°C) for 15 min and then in 4% freshly prepared paraformaldehyde for 5 min. Endogenous peroxidase activity was blocked by incubation for 15 min in phosphate-buffered saline (PBS) supplemented by 1% H_2O_2 and 0.1% sodium azide. Endogenous biotin was blocked by means of a DakoCytomation blocking kit (DakoCytomation, Denmark). In order to block nonspecific binding, sections were treated with 3% BSA in PBS for 15 min. GM1 ganglioside was detected in liver sections using CTB biotin labelled (Sigma, USA), diluted 1:300 in PBS, plus 3% BSA at 8°C for 16.5 h, followed with streptavidin-peroxidase polymer at room temperature for 1 h. Peroxidase activity was visualized with diaminobenzidine tetrahydrochloride for 20 min in the dark. Sections were mounted in mounting medium Dako S3025 (Dako North America, CA, USA).

Two negative control tests were performed for each group. First, CTB was omitted in immunohistochemical staining. Second, fixed sections were extracted with chloroform : methanol 2:1 at room temperature for 30 minutes followed by standard immunohistochemical staining.

2.6. Densitometric Analysis of GM1 Ganglioside in Sinusoidal Membrane and Adjacent Cytoplasm Areas. Six liver specimens were used from each animal. One section from each specimen was used for GM1 ganglioside detection with CTB as described above. From each section, four hepatic lobules with a clearly discernible central vein were selected. In each lobule, one measuring frame in the central lobular zone III and one measuring frame in the corresponding peripheral lobular zone I were selected for analysis. In each frame, 15 areas of sinusoidal surface and 15 areas of adjacent hepatocyte cytoplasm were selected by the stratified random sampling method [24] and marked out. The reaction product was quantified as the mean optical density of the analyzed areas (determined by the densitometric program ACC 6.0, SOFO, Czech Republic) at objective magnification of 40x (NA = 0.7). The ratios of densities measured in the sinusoidal membrane and subsinusoidal intracellular compartment were measured and compared together (sin/int).

2.7. Cell Culture Experiments. Human neuroblastoma cell line SH-SY5Y (ATCC, Manassas, VA, USA) was cultured in the Minimum Essential Medium Eagle (MEM) and Ham's F-12 medium (1:1, *v*/*v*) with 15% of fetal bovine serum and human hepatoblastoma cell line HepG2 (ATCC, Manassas, VA, USA) in MEM with 10% of fetal bovine serum in a humidified atmosphere (containing 5% CO_2 and 37°C). Authentication of used cell lines was confirmed by an independent laboratory using a method based on an accredited short tandem repeat analysis.

Cells were seeded onto 6-well plates (Corning, NY, USA) at a concentration of 50,000 cells per 1 cm^2 and treated with CDCA and bilirubin for 4 h. SH-SY5Y cells were also treated with PKC activator (phorbol 12-myristate 13-acetate) or PKC inhibitor (Ro 31-0432) for 4 h. After the incubation period, cells were harvested into the lysis buffer and stored at −80°C for further experiments.

2.8. Measurement of Intracellular ROS Production. ROS production was determined using a fluorescent probe 5-(and-6)-chloromethyl-2′,7′-dichlorodihydrofluorescein diacetate acetyl ester (CM-H_2DCFDA, Life Technologies, USA). Briefly, SH-SY5Y cells were grown in 12-well plates to 80% confluence. Cells were then incubated with CDCA and/or antioxidant (bilirubin) for 24 h. After the incubation, the cells were washed twice with PBS and loaded with 10 μM CM-H2DCFDA at 37°C for 30 min in the dark, then washed with PBS to remove excess dye. Fluorescence was measured using 485 nm excitation and 540 nm emission wavelengths in microplate reader (Synergy HTX, BioTek, USA). Cells were then lysed with Cell Lysis Buffer (Cell Signaling Technology, USA), and protein concentration was measured using DC Protein Assay (Bio-Rad, USA) according to the manufacturer's instruction. Data were normalized to protein content and expressed as % of controls.

2.9. Lipid Peroxidation. Lipid peroxidation was measured according to the method by Vreman et al. [31]. Twenty microliters of 10% liver or brain sonicates in 0.1 M phosphate buffer, pH = 7.4, were incubated at 37°C with 100 μM ascorbate (80 μL) and 6 μM Fe^{2+} (0.5 μL) in a septum-sealed vial. Butylated hydroxytoluene (10 μM) was added to the blank reaction. The reaction was terminated by adding 2 μL of 60% sulfosalicylic acid. CO produced into the vial headspace was quantified by gas chromatography with a reduction gas analyzer (Peak Laboratories LLC, Mountain View, CA, USA). The amount of CO produced served as an index of lipid peroxidation, was measured as picomoles of CO per hour per milligram of fresh tissue, and was expressed as % of control.

2.10. Western Blotting. Cells grown to 60% confluency were lysed using RIPA buffer supplemented with phosphatase and protease inhibitors (Protease Inhibitor Mix G and Phosphatase Inhibitor Mix I, Serva, Heidelberg, Germany). Samples were separated by SDS-PAGE on 12% polyacrylamide gel and then transferred to nitrocellulose membrane (Bio-Rad Laboratories, Hercules, CA, USA). After blocking in Tween-PBS with 5% BSA (Sigma-Aldrich, St. Louis, MO, USA) for at least 1.5 h, membranes were incubated with GM3 synthase and GM2/GD2 synthase antibody (1:2000; Santa Cruz sc-365329 and sc-376505, Dallas, TX, USA), or β-actin (1:2000; Cell Signaling Technology, Danvers, MA, USA) overnight at 4°C. After washing, membranes were incubated with anti-mouse m-IgGκ BP-HRP (Santa Cruz

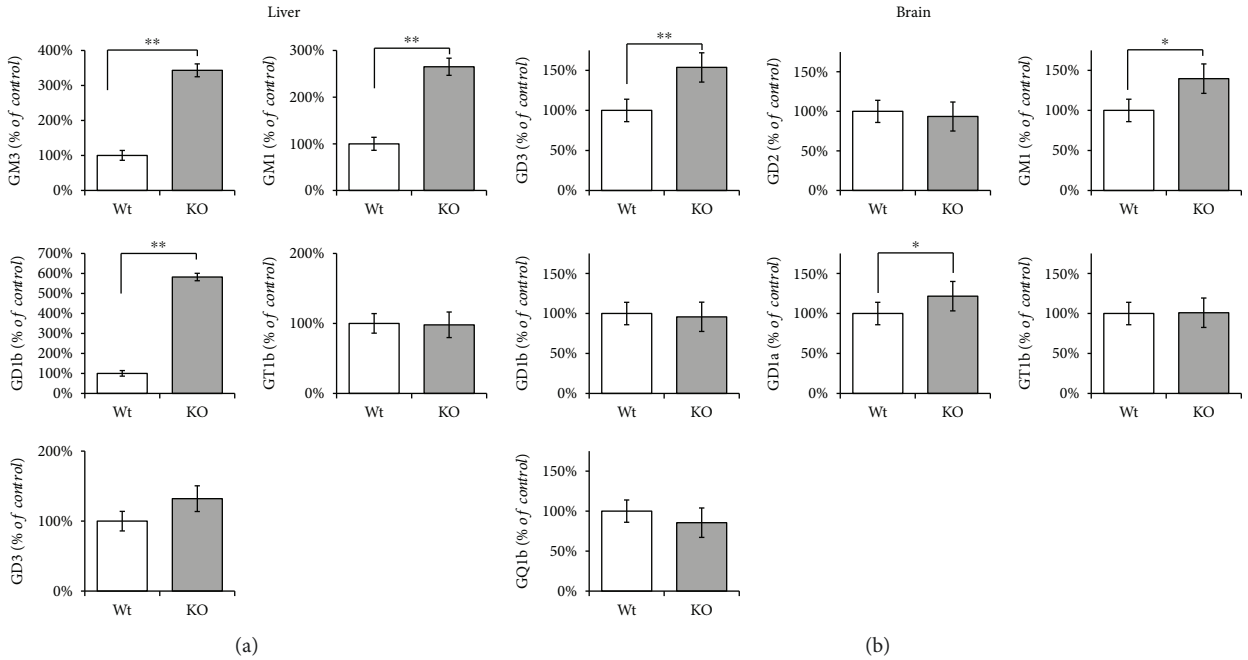

Figure 1: The impact of *Hmox1* knockout on ganglioside composition in mouse (a) liver and (b) brain. Isolated hepatic (a) and brain (b) gangliosides were separated in a solvent system and analyzed by a densitometric method after TLC separation and detection using resorcinol-HCl reagent. Values are expressed as % of control and represent mean SD. Wt: wild-type ($n = 6$); KO: *Hmox1* knockout ($n = 9$). $^{*}P < 0.05$ and $^{**}P < 0.01$.

sc-516102, Dallas, TX, USA) for 1 h. Immunocomplexes on the membranes were visualized with ECL Western Blotting Detection Reagents (Cell Signaling Technology) using an Odyssey infrared imaging system (LI-COR Biosciences, Lincoln, NE, USA).

2.11. Quantitative Real-Time PCR. The liver samples were stored frozen at −80°C in RNAlater (Sigma-Aldrich, St. Louis, USA), and total RNA was isolated using a Qiagen RNAeasy Plus kit and QIAshredder (Qiagen, USA). Cell culture samples were stored in lysis buffer at −80°C, and total RNA was isolated using PerfectPure RNA Cell Kit (5Prime, USA). A High-Capacity cDNA Reverse Transcription Kit (Life Technologies, Carlsbad, CA, USA) was used to generate cDNA. Quantitative real-time PCR was performed using TaqMan® Gene Expression Assay Kit (Life Technologies, Carlsbad, CA, USA) for the following genes: *GlcT* (Hs00234293_m1), *GalTI* (Hs00191135_m1), GM3 synthase (*St3GalV*, Mm00488237_m1, and Hs01105379_m1), GD3 synthase (*STSia8*, Mm00456915_m1, and Hs00268157_m1), GM2/GD2 synthase (*B4GalNT1*, Mm00484653_m1, and Hs01110791_g1), and GM1 synthase (*B3GalT4*, Mm00546324_s1, and Hs00534104_s1), all provided by Life Technologies (Carlsbad, CA, USA). The data were normalized to HPRT and expressed as percent of control levels.

2.12. Statistical Analysis. Normally distributed data are presented as mean ± SD and analyzed by the Student t-test. The Mann–Whitney U test or Kruskal-Wallis test were used in skewed data. Differences with $P < 0.05$ were considered significant.

3. Results

3.1. The Impact of Hmox1 Knockout on the Liver and Brain Ganglioside Content. To investigate the role of *Hmox1* knockout on the ganglioside pattern, we measured changes in ganglioside composition in the liver as well as the brain, the tissue with the highest glycolipid content *in vivo*. As the ganglioside spectra differ within specific tissues, only major gangliosides and representatives of two main biosynthetic pathways, *a*- and *b*-series, were determined.

In the liver, mice lacking *Hmox1* exhibited marked increases in the concentrations of individual gangliosides. Specifically, *Hmox1* knockout led to a significant increase in GM3 (343 ± 76%, $P < 0.001$) and GM1 (265 ± 62%, $P < 0.001$) representing *a*-series, and GD1b (582 ± 176%, $P < 0.001$) from *b*-series of gangliosides (Figure 1(a)).

In the brain, the most abundant ganglioside was GD1a in both wild-type as well as knockout animals. Together with GM1, GD1a content was significantly higher (GD1a 122% vs. Wt, $P < 0.05$; GM1 140% vs. Wt, $P < 0.05$) in *Hmox1* knockout mice as compared to wild types. The other two major brain gangliosides (GM3, GT1b) stayed unchanged after *Hmox1* knockout. The amount of minor GD3 ganglioside was also significantly increased (154% vs. Wt, $P < 0.01$) (Figure 1(b)). The scheme of de novo biosynthesis of the oligosaccharide moieties of gangliosides is illustrated in Figure 2.

To confirm the level of oxidative stress in *Hmox1* knockouts, we measured the extent of lipid peroxidation in liver and brain tissue homogenates. Importantly, liver lipid peroxidation was increased in *Hmox1* knockout mice as compared to controls (155% ± 51% $Hmox^{-/-}$, $n = 7$, vs. 100% ± 46%

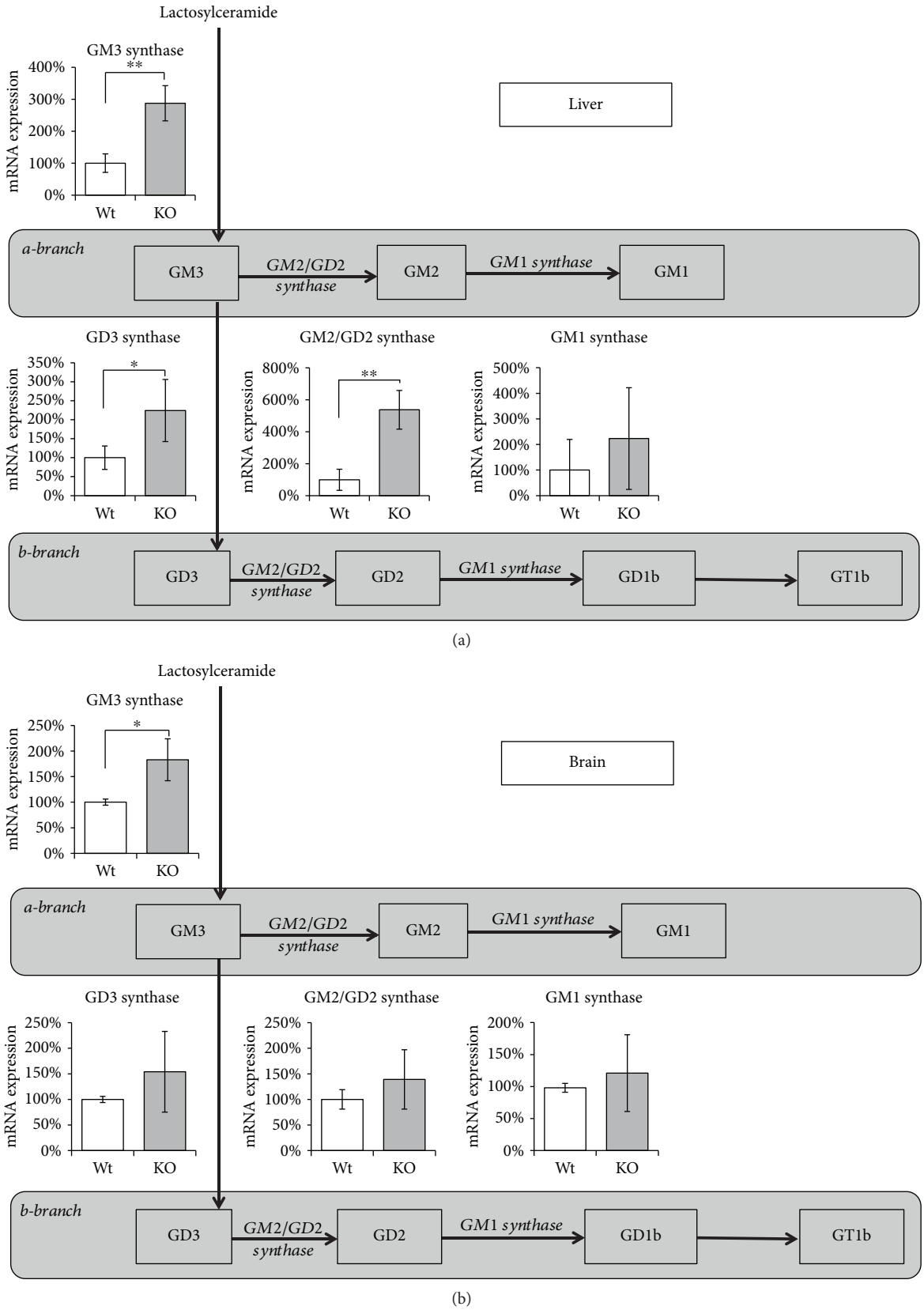

Figure 2: *Hmox1* knockout leads to changes in sialyltransferase expression in the liver and brain. Relative mRNA expression of the key enzymes in ganglioside synthesis was measured in the liver (a) and brain (b) tissues of wild-type (Wt) and *Hmox1* knockout (KO) animals. Values are expressed as % of control. Wt: wild-type ($n = 6$); KO: *Hmox1* knockout ($n = 9$). $^{*}P < 0.01$; $^{**}P < 0.001$.

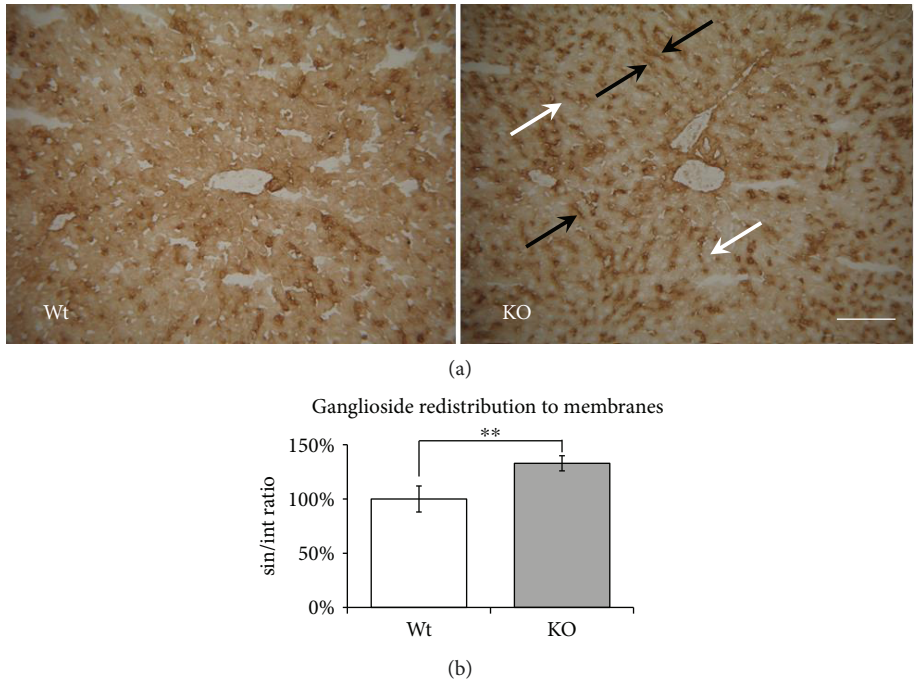

Figure 3: The effect of *Hmox1* knockout on distribution/localization of GM1 ganglioside in the liver. (a) Immunohistochemical detection of GM1 ganglioside. In the liver sections, GM1 ganglioside was detected using the cholera toxin B subunit with streptavidin-peroxidase polymer. Diaminobenzidine tetrahydrochloride (brown colour) was used for visualization. The shift of GM1 ganglioside expression from intracellular localization (white arrows) into sinusoidal membranes (black arrows) was observed in *Hmox1* knockout animals. (b) Quantification of GM1 staining in the liver. Image analysis of the distribution of GM1 ganglioside staining in the subsinusoidal part of the intracellular compartment (int) and sinusoidal membranes (sin) of hepatocytes, expressed as the sin/int ratio relative to control (Wt). The reaction product was quantified as the mean optical density of the analyzed areas at objective magnification of 40x (NA = 0.7). Bar represents 100 μm. Wt: wild-type ($n = 6$); KO: *Hmox1* knockout ($n = 9$). $^{**}P < 0.01$.

$Hmox^{+/+}$, $n = 6$, $P = 0.032$). No significant increase was observed in a brain tissue (115% ± 46% $Hmox^{-/-}$, $n = 7$, vs. 100% ± 45% $Hmox^{+/+}$, $n = 6$, $P = 0.311$).

3.2. Hmox1 Knockout Results in Changes in the Expression of Sialyltransferases. Relative mRNA expression of the key sialyltransferases was determined to elucidate the activation rate of *a*- and *b*-series of a ganglioside biosynthetic pathway in mouse liver and brain homogenates. *Hmox1* knockout led to a significant increase in mRNA expression of GM3 synthase (*ST3GalV*) (287 ± 55%, $P < 0.001$; 183 ± 41%, $P < 0.01$) in both liver and brain, and GD3 synthase (*St8SiaI*) (224 ± 89%, $P < 0.01$), the key step in an activation of *b*-biosynthetic branch in the liver. *Hmox1* knockout caused also significant activation of GM2/GD2 synthase (*B4GalNTI*) (538 ± 121%, $P < 0.001$) in the liver. Expression of GM1 synthase (*B3GalTIV*) stayed unchanged in both liver and brain (Figure 2).

3.3. Hmox1 Knockout Leads to a Marked Shift of Gangliosides to the Hepatocyte Membrane. To study possible changes in distribution of gangliosides within mouse hepatocytes, histochemical localization of GM1, the representative of gangliosides, was determined in the liver sections. In control liver specimens, GM1 was detected in both sinusoidal and canalicular membranes, as well as in the intracytoplasmic compartment. In *Hmox1* knockout animals, we observed a pronounced shift in GM1 ganglioside expression from intracellular localization into sinusoidal membranes (Figure 3(a)). To quantify this redistribution pattern of GM1, we measured the GM1 expression under high microscopic magnification expressed as sin/int ratio (GM1 staining in the sinusoidal membrane/subsinusoidal intracellular compartment) (133 ± 7%, $P < 0.01$, Figure 3(b)).

3.4. Ganglioside Pattern in Neuroblastoma Cells (SH-SY5Y) Is Affected by Oxidative Stress. To find out whether changes in the ganglioside pattern might be affected by an increased oxidative stress associated with *Hmox1* knockout, we investigated the regulation of glycosphingolipid (GSL) synthesis using SH-SY5Y neuroblastoma cells rich in gangliosides. CDCA, a potent inducer of ROS production accumulating in the liver during cholestasis, was used to increase oxidative stress *in vitro*, while addition of bilirubin, a potent antioxidant and a product of the Hmox pathway, had an opposite effect (Figure 4).

Administration of CDCA (80 μM) resulted in a significant increase in the major gangliosides GD1a (141%, $P < 0.01$), GM3 (170%, $P < 0.01$), and GM2 (130%, $P < 0.05$) in SH-SY5Y neuroblastoma cells (Figure 5(a)) and GM3 (233%, $P < 0.01$) and GM2 (251%, $P < 0.05$) in hepatoblastoma HepG2 cells (Figure 5(b)). Interestingly, coadministration of bilirubin (CDCA/bilirubin), a potent antioxidant, resulted in normalization of the ganglioside pattern in both cell lines (Figure 5).

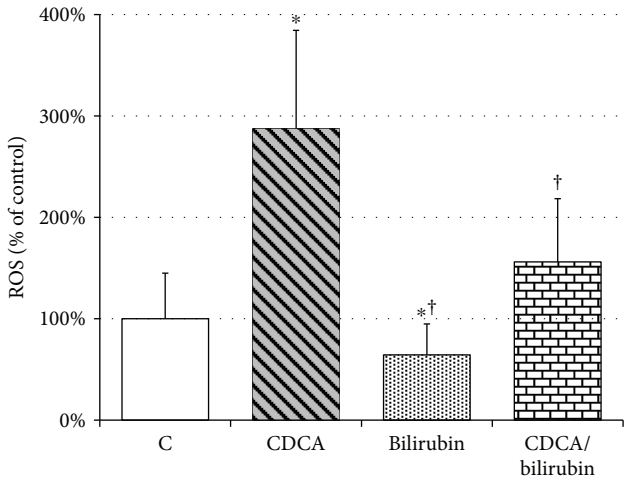

Figure 4: The ameliorating effect of bilirubin on CDCA-induced oxidative stress in SH-SY5Y cells. SH-SY5Y cells were incubated with CDCA (80 μM), bilirubin (1 μM), or both (CDCA/bilirubin) for 24 h. ROS production was measured using fluorescent CM-H2DCFDA probe. Values are expressed as % of controls. C: control; CDCA: chenodeoxycholic acid (80 μM); bilirubin: 1 μM bilirubin; CDCA/bilirubin: CDCA (80 μM) + bilirubin (1 μM). $^{*}P < 0.05$ vs. C; $^{\dagger}P < 0.05$ vs. CDCA.

3.5. Oxidative Stress-Mediated Changes in Sialyltransferase (ST3GalV) Expression Are Regulated through the Protein Kinase C Pathway. To elucidate whether oxidative stress induced by CDCA affects the expression of GM3 synthase (*ST3GalV*), a key enzyme in ganglioside metabolism, *in vitro*, SH-SY5Y as well as HepG2 cell lines were incubated with CDCA and/or bilirubin for 4 h. Significant increases in GM3 synthase mRNA expression were observed upon CDCA treatment while cotreatment with bilirubin abolished this effect in both neuroblastoma (Figure 6(a)) and hepatic (Figure 6(c)) cell lines. The results were confirmed by the detection of GM3 synthase protein expression in the SH-SY5Y cell line (Figure 6(b)).

To investigate the possible role of the PKC pathway on oxidative stress-mediated changes in ganglioside expression, we measured the effect of PKC induction/inhibition ($PKC^{+/-}$) on the mRNA expression of *GM3 synthase* (*ST3GalV*), in the SH-SY5Y cell line. PKC activators induced the mRNA expression of *ST3GalV*. On the other hand, PKC inhibitors significantly decreased *ST3GalV* mRNA expression. Importantly, cotreatment of CDCA with PKC inhibitor completely abolished the stimulatory effect of CDCA on *ST3GalV* mRNA (Figure 6(d)). Successful PKC activation and/or inhibition was proven by determination of mRNA expression of PKC alpha, PKC beta, and PKC epsilon (Figure 6(e)).

4. Discussion

Gangliosides play a crucial role in signal transduction pathways, regulating many different cell functions such as proliferation, differentiation, adhesion, and cell death [32, 33]. They are responsible for the rigidity of a plasmatic membrane [34] and participate in a protection against oxidative stress [19, 21]. However, the significance of changes in ganglioside metabolism under oxidative stress remains to be elucidated. To address this issue, we have studied the consequences of the antioxidant enzyme Hmox1 deficiency for ganglioside metabolism in mouse tissues. Unlike in the brain, we found significantly increased lipid peroxidation in the liver of *Hmox1* knockout animals which is in accordance with the published data showing increased lipid peroxidation and hepatic injury mostly due to iron accumulation in the liver tissue [6]. Our results indicate that oxidative stress plays an important role in ganglioside synthesis resulting in changes in their spectra and cellular distribution.

Gangliosides are ubiquitously found in tissues and body fluid with the most abundant expression in the nervous system [35]. The expression levels of gangliosides undergo dramatic changes during various physiological and pathological conditions including cell death, proliferation, differentiation, development, and oncogenesis [36–38] as well as neurological diseases [39, 40]. These effects are largely attributed to the changes in expression levels of ganglioside synthases (glycosyltransferases) [41, 42]. In our previous experiments on rats, we observed the shift in liver ganglioside synthesis towards more complex ones in various types of cholestatic liver diseases [25, 30]. These changes were associated with the accumulation of detergent and prooxidative bile acids as well as with the increase in oxidative stress in these animals [21, 22].

In the present study, *Hmox1* knockout resulting in the absence of an important antioxidant enzyme in experimental mice was accompanied by significant increases in the brain GM1, GD1a, and GD3 and liver GM1, GM3, and GD1b gangliosides. The tissue specificity of these changes might be explained by the different ganglioside composition of the liver and brain tissues. While GM3 is the main ganglioside in the liver, GD1a is the most abundant in the adult brain [38, 43], where GD1a, GM1, GD1b, GT1b, and GD3 belong to most important glycosphingolipids [44]. Several reports suggest gangliosides to possess antioxidant properties, but very little is known about the function of gangliosides in the liver and therefore most data relates to the nervous tissue [11]. Among these, GM1 ganglioside has neuroprotective functions. Micelles containing GM1 inhibited iron-catalysed hydroxyl radical formation *in vitro* [18], GM1 decreased ROS formation in rat brain synaptosomes [45], or protected cells against H_2O_2-induced oxidative damage [46] while GD1b was able to inhibit lipid peroxidation in human sperm cells [47]. On the other hand, some gangliosides might enhance ROS formation and contribute to the cell death. Sohn et al. [48] found GM3, but not GD3 or GT1b, to mediate oxidative toxicity induced by glutamate in immortalized mouse neuronal HT22 cells. GD3 was described to interact with mitochondria and generate ROS [49, 50], and there is strong evidence for involvement of GD3 in autophagosome formation [51, 52]. GD3 is also considered a key player in apoptosis by Fas, ceramide, and amyloid-β [53, 54]. These findings suggest an important role of gangliosides in processes involved in oxidative stress regulation which might explain their compensatory upregulation in the prooxidative environment of *Hmox1* knockout.

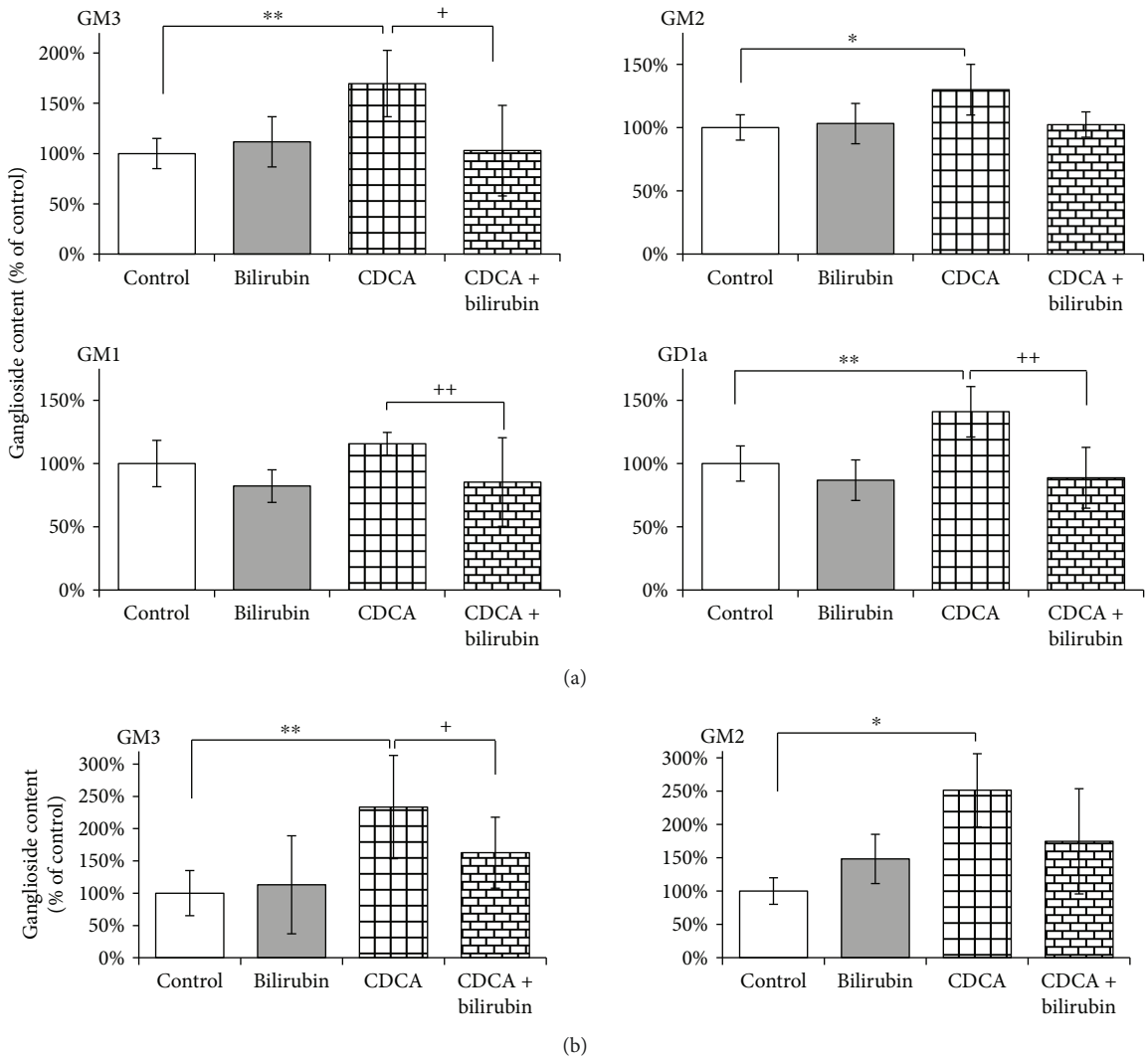

Figure 5: The ameliorating effect of bilirubin on CDCA-induced change in ganglioside content in SH-SY5Y cells (a) and HepG2 cells (b). Relative content of individual gangliosides was evaluated using extraction and TLC densitometry after incubation with CDCA or CDCA/bilirubin for 4 in (a) SH-SY5Y cells and (b) HepG2 cells. Values are expressed as % of controls. Bilirubin (1 μM); CDCA: chenodeoxycholic acid (80 μM); CDCA/bilirubin: CDCA (80 μM) + bilirubin (1 μM). $^{*}P < 0.05$ vs. C; $^{**}P < 0.01$ vs. C; $^{+}P < 0.05$ vs. CDCA; $^{++}P < 0.01$ vs. CDCA.

The effect of oxidative stress on changes in ganglioside synthesis was further supported by determination of glycosyltransferase mRNA expressions in mouse liver and brain homogenates. The key regulatory enzymes in the synthesis of nearly all gangliosides, *GM3* and *GD3 synthases*, as well as *GalNAcT*, were found to be significantly increased in *Hmox1* knockouts while GM1 synthase expression stayed unchanged. These data correspond with the observed increases in liver gangliosides and are in accordance with our previous observations on liver glycosyltransferase expression in experimental cholestasis in rats [22]. The increase in liver GM1 ganglioside content in *Hmox1* knockouts allows speculating that expression of *GM1 synthase* is redundant in wild-type animals and is capable of maintaining the induction of the *GalNAcT* product. Interestingly, only GM3 synthase has been found to be significantly upregulated in the brain suggesting the tissue-specific regulation of various sialyltransferases. Moreover, different extents of oxidative stress in particular tissues might affect the final sialyltransferase expression.

Furthermore, in our earlier reports, we described not only an increase in ganglioside synthesis but also their shift into the sinusoidal membranes of hepatocytes upon oxidative stress induced by bile acids [21]. This mechanism could protect hepatocytes against detergent and prooxidant effects of bile acids. A very similar effect was observed in the present study. We have used a selective histochemical approach based on the high binding affinity of *Cholera toxin* B subunit to GM1 ganglioside [6], the representative of the complex gangliosides. A significant shift of GM1 gangliosides from intracellular localization to the membrane compartment was found in *Hmox1* knockout which is also associated with prooxidative condition.

To investigate the mechanism of oxidative stress-mediated changes in ganglioside metabolism, we used the *in vitro* model of the SH-SY5Y neuroblastoma cell line rich

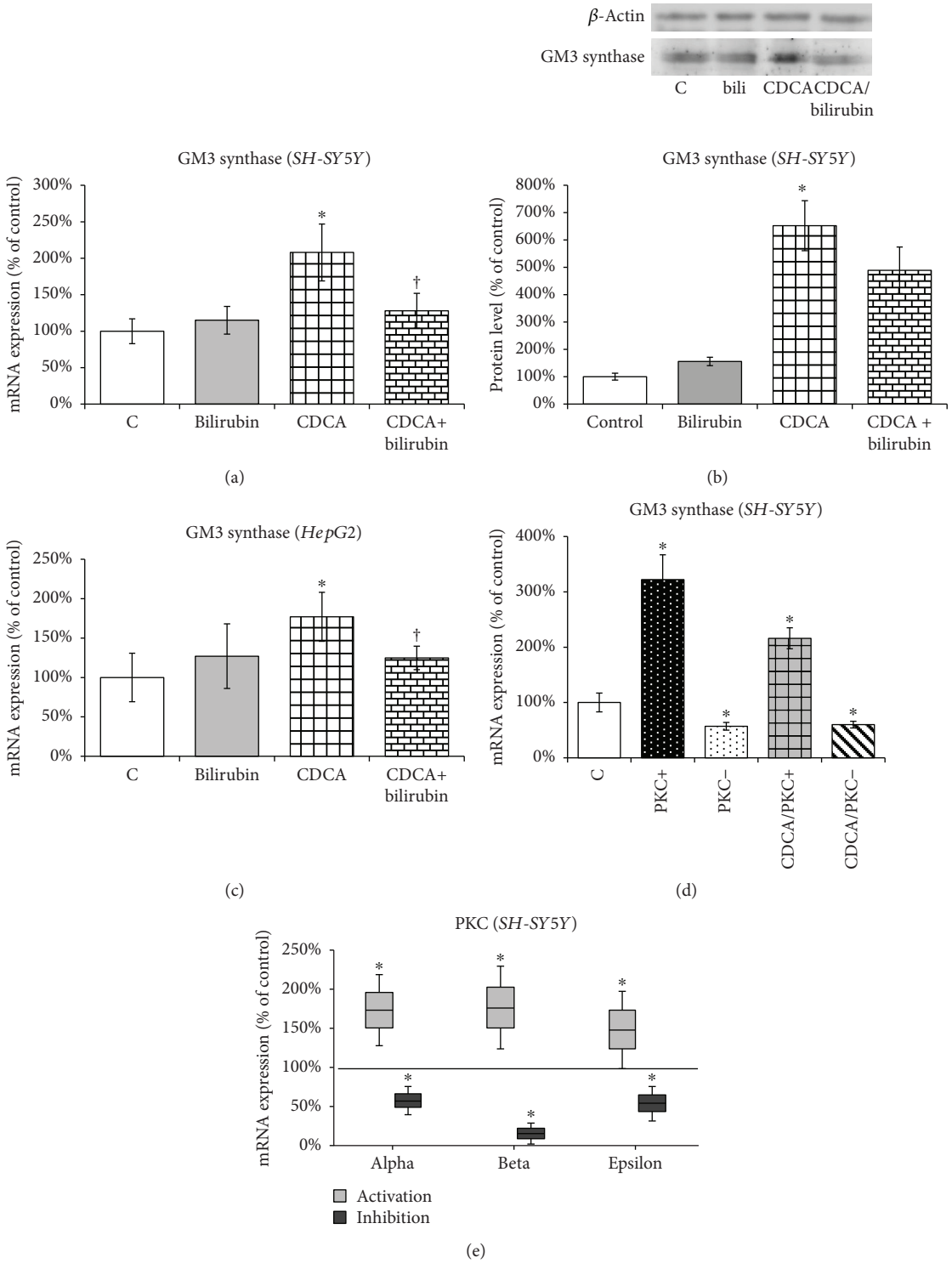

Figure 6: The opposite effects of CDCA and bilirubin on regulation of GM3 synthase expression in SH-SY5Y and HepG2 cells. (a) Relative GM3 synthase (ST3GalV) mRNA expression was determined in control cells (C), after 4 h incubation with chenodeoxycholic acid (CDCA) and/or bilirubin in SH-SY5Y cells. (b) Relative GM3 synthase (ST3GalV) protein expression by Western blot was determined in control cells (C), after 4 h incubation with chenodeoxycholic acid (CDCA) and/or bilirubin in SH-SY5Y cells. (c) Relative GM3 synthase (ST3GalV) mRNA expression was determined in control cells (C), after 4 h incubation with chenodeoxycholic acid (CDCA) and/or bilirubin in HepG2 cells. (d) PKC activity was modulated by incubating SH-SY5Y cells with PKC activator (PKC^+) or PKC inhibitor (PKC^-) or their combination with CDCA ($CDCA/PKC^+$, $CDCA/PKC^-$) for 4 h. (e) PKC activation and/or inhibition was proven by determination of mRNA expression vs. control (100% line) of PKC alpha, PKC beta, and PKC epsilon in SH-SY5Y cells. Values are expressed as % of controls. C: control; PKC^+: PKC activation by phorbol 12-myristate 13-acetate (5 μM); PKC^-: PKC inhibition by Ro 31-0432 (5 μM); CDCA: chenodeoxycholic acid (80 μM); CDCA/bilirubin: CDCA (80 μM) + bilirubin (1 μM). $^*P < 0.05$ vs. C; $^\dagger P < 0.05$ vs. CDCA.

in glycosphingolipids and, for the comparison, the human hepatoblastoma HepG2 cell line. Interestingly, the HepG2 cell line was found to be very poor in ganglioside content and completely lacking GD3 synthase. Exposure of SH-SY5Y to oxidative stress induced by chenodeoxycholic acid [55] resulted in a significant increase in all major gangliosides of this cell line—GD1a, GM3, and GM2—while addition of a potent antioxidant, bilirubin [56], resulted in normalization of the ganglioside content. Importantly, the same pattern was observed in the HepG2 cell line in GM3 and GM2 gangliosides. These results are in accordance with our earlier observations [10] that bilirubin may counteract a prooxidative effect of BA on hepatocytes in the model of obstructive cholestasis in rats. Furthermore, accumulation of hydrophobic BA in the brain and their possible involvement in hepatic encephalopathy associated with cholestatic liver diseases has been reported [57]. BA can act as cell signalling effectors through binding and activating receptors on both the cell membrane and nucleus. BA signalling encompasses both direct (FXR, TGR5) and indirect (FGF19, GLP-1) pathways. The role of BA in extrahepatic diseases is becoming more important, and increasing amount of reports suggests that BA might play an important role in neurological function and diseases [58, 59].

To elucidate the mechanism of oxidative stress-induced changes of ganglioside metabolism, we focused on regulation of the main enzyme in complex ganglioside synthesis, GM3 synthase (*ST3GalV*).

PKC appeared to be a logical candidate regulating the expression of GM3 synthase. Hydrophobic bile acids are considered potent inducers of PKC while antioxidants inhibit PKC activity [60, 61]. For more than 30 years, it has been known that ganglioside metabolism is in tight connection to PKC activity [62–64], and the action of glycosyltransferases is controlled through posttranslational modification. Glycosyltransferase activities have been demonstrated to be significantly modulated by the action of PKC [65]. Another study suggested the role of PKC as an activator of GM3 synthase (*ST3GalV*) [66]. Our *in vitro* data support this hypothesis. While PKC activators and oxidative stress induced the expression of *ST3GalV*, PKC inhibitors as well as antioxidants completely abolished this effect.

There are some limitations of our study. First, we were primarily interested in the shift of GSL to the cytoplasmic membrane; however, more studies are needed to assess whether subcellular localization and trafficking of gangliosides are affected as well. Second, in histochemical analyses, we used GM1 as a GSL representative but further studies with individual gangliosides are needed to confirm that the shift of GM1 from the intracellular compartment to the cytoplasmic membrane is a general reaction to loss of Hmox1 action. Finally, the PKC pathway is an important but probably not the only pathway regulating GSL metabolism affected by oxidative stress.

5. Conclusions

We conclude that oxidative stress is an important factor modulating synthesis and distribution of gangliosides *in vivo* and *in vitro*. Knockout of *Hmox1*, an important antioxidant enzyme, results in tissue-specific increases in main gangliosides together with changes in mRNA expression of key enzymes of ganglioside synthesis. We demonstrate that these changes might be, at least partially, mediated through modulation of the PKC pathway.

Data Availability

The raw data used to support the findings of this study are available from the corresponding author upon request.

Conflicts of Interest

The authors declare that there is no conflict of interest regarding the publication of this paper.

Acknowledgments

The study was supported by Grant RVO-VFN64165/2018 given by the Czech Ministry of Health; PROGRES Q25/LF1, GAUK 516912, and SVV 260370-2017 provided by the Charles University, Prague, Czech Republic; and the statutory funds from the Jagiellonian University. The Faculty of Biochemistry, Biophysics and Biotechnology of Jagiellonian University is a partner of the Leading National Research Centre (KNOW) supported by the Ministry of Science and Higher Education. The authors wish to thank Janusz Drebot and Witold Nowak for their help with the animal experiments, Kateřina Žížalová for her help with cell culture experiments, and Olga Švejdová and Marie Kolářová for their excellent technical assistance.

References

[1] L. E. Otterbein, M. P. Soares, K. Yamashita, and F. H. Bach, "Heme oxygenase-1: unleashing the protective properties of heme," *Trends in Immunology*, vol. 24, no. 8, pp. 449–455, 2003.

[2] P. Ayuso, C. Martínez, P. Pastor et al., "An association study between *Heme oxygenase-1* genetic variants and Parkinson's disease," *Frontiers in Cellular Neuroscience*, vol. 8, p. 298, 2014.

[3] H. Schipper and W. Song, "A heme oxygenase-1 transducer model of degenerative and developmental brain disorders," *International Journal of Molecular Sciences*, vol. 16, no. 12, pp. 5400–5419, 2015.

[4] L. E. Fredenburgh, A. A. Merz, and S. Cheng, "Haeme oxygenase signalling pathway: implications for cardiovascular disease," *European Heart Journal*, vol. 36, no. 24, pp. 1512–1518, 2015.

[5] K. D. Poss and S. Tonegawa, "Reduced stress defense in heme oxygenase 1-deficient cells," *Proceedings of the National Academy of Sciences of the United States of America*, vol. 94, no. 20, pp. 10925–10930, 1997.

[6] S. T. Fraser, R. G. Midwinter, B. S. Berger, and R. Stocker, "Heme oxygenase-1: a critical link between iron metabolism, erythropoiesis, and development," *Advances in Hematology*, vol. 2011, Article ID 473709, 6 pages, 2011.

[7] T. Mamiya, F. Katsuoka, A. Hirayama et al., "Hepatocyte-specific deletion of heme oxygenase-1 disrupts redox homeostasis in basal and oxidative environments," *The Tohoku Journal of Experimental Medicine*, vol. 216, no. 4, pp. 331–339, 2008.

[8] L. Novotny and L. Vitek, "Inverse relationship between serum bilirubin and atherosclerosis in men: a meta-analysis of published studies," *Experimental Biology and Medicine*, vol. 228, no. 5, pp. 568–571, 2003.

[9] J. Zelenka, L. Muchova, M. Zelenkova et al., "Intracellular accumulation of bilirubin as a defense mechanism against increased oxidative stress," *Biochimie*, vol. 94, no. 8, pp. 1821–1827, 2012.

[10] L. Muchova, K. Vanova, J. Zelenka et al., "Bile acids decrease intracellular bilirubin levels in the cholestatic liver: implications for bile acid-mediated oxidative stress," *Journal of Cellular and Molecular Medicine*, vol. 15, no. 5, pp. 1156–1165, 2011.

[11] R. K. Yu, Y. Nakatani, and M. Yanagisawa, "The role of glycosphingolipid metabolism in the developing brain," *Journal of Lipid Research*, vol. 50, pp. S440–S445, 2009.

[12] A. Regina Todeschini and S. I. Hakomori, "Functional role of glycosphingolipids and gangliosides in control of cell adhesion, motility, and growth, through glycosynaptic microdomains," *Biochimica et Biophysica Acta (BBA) - General Subjects*, vol. 1780, no. 3, pp. 421–433, 2008.

[13] H. Rahmann, "Brain gangliosides and memory formation," *Behavioural Brain Research*, vol. 66, no. 1-2, pp. 105–116, 1995.

[14] B. Wang, "Sialic acid is an essential nutrient for brain development and cognition," *Annual Review of Nutrition*, vol. 29, no. 1, pp. 177–222, 2009.

[15] L. J. Pike, "Rafts defined: a report on the keystone symposium on lipid rafts and cell function," *Journal of Lipid Research*, vol. 47, no. 7, pp. 1597-1598, 2006.

[16] D. Lingwood and K. Simons, "Lipid rafts as a membrane-organizing principle," *Science*, vol. 327, no. 5961, pp. 46–50, 2010.

[17] J. Taira, M. Sugishima, Y. Kida, E. Oda, M. Noguchi, and Y. Higashimoto, "Caveolin-1 is a competitive inhibitor of heme oxygenase-1 (HO-1) with heme: identification of a minimum sequence in caveolin-1 for binding to HO-1," *Biochemistry*, vol. 50, no. 32, pp. 6824–6831, 2011.

[18] M. Gavella, M. Kveder, V. Lipovac, D. Jurašin, and N. Filipovi-Vinceković, "Antioxidant properties of ganglioside micelles," *Free Radical Research*, vol. 41, no. 10, pp. 1143–1150, 2007.

[19] M. Gavella, M. Kveder, and V. Lipovac, "Modulation of ROS production in human leukocytes by ganglioside micelles," *Brazilian Journal of Medical and Biological Research*, vol. 43, no. 10, pp. 942–949, 2010.

[20] N. F. Avrova, I. V. Victorov, V. A. Tyurin et al., "Inhibition of glutamate-induced intensification of free radical reactions by gangliosides: possible role in their protective effect in rat cerebellar granule cells and brain synaptosomes," *Neurochemical Research*, vol. 23, no. 7, pp. 945–952, 1998.

[21] T. Petr, V. Smíd, V. Kučerová et al., "The effect of heme oxygenase on ganglioside redistribution within hepatocytes in experimental estrogen-induced cholestasis," *Physiological Research*, vol. 63, no. 3, pp. 359–367, 2014.

[22] V. Šmíd, T. Petr, K. Váňová et al., "Changes in liver ganglioside metabolism in obstructive cholestasis - the role of oxidative stress," *Folia Biologica*, vol. 62, no. 4, pp. 148–159, 2016.

[23] A. Szade, W. N. Nowak, K. Szade et al., "Effect of crossing C57BL/6 and FVB mouse strains on basal cytokine expression," *Mediators of Inflammation*, vol. 2015, Article ID 762419, 10 pages, 2015.

[24] P. W. Hamilton, "Designing a morphometric study," in *Quantitative Clinical Pathology*, P. W. Hamilton and D. C. Allen, Eds., Blackwell Science, Cambridge, MA, USA, 1995.

[25] F. Majer, L. Trnka, L. Vítek, M. Jirkovská, Z. Mareček, and F. Šmíd, "Estrogen-induced cholestasis results in a dramatic increase of b-series gangliosides in the rat liver," *Biomedical Chromatography*, vol. 21, no. 5, pp. 446–450, 2007.

[26] R. K. Yu and R. W. Ledeen, "Gangliosides of human, bovine, and rabbit plasma," *Journal of Lipid Research*, vol. 13, no. 5, pp. 680–686, 1972.

[27] K. Suzuki, "The pattern of mammalian brain gangliosides-II evaluation of the extraction procedures, postmortem changes and the effect of formalin preservation," *Journal of Neurochemistry*, vol. 12, no. 7, pp. 629–638, 1965.

[28] J. Folch, M. Lees, and G. H. Sloane Stanley, "A simple method for the isolation and purification of total lipides from animal tissues," *The Journal of Biological Chemistry*, vol. 226, no. 1, pp. 497–509, 1957.

[29] M. A. Chester, "IUPAC-IUB Joint Commission on Biochemical Nomenclature (JCBN). Nomenclature of glycolipids—-recommendations 1997," *European Journal of Biochemistry*, vol. 257, no. 2, pp. 293–298, 1998.

[30] M. Jirkovská, F. Majer, J. Šmídová et al., "Changes in GM1 ganglioside content and localization in cholestatic rat liver," *Glycoconjugate Journal*, vol. 24, no. 4-5, pp. 231–241, 2007.

[31] H. J. Vreman, R. J. Wong, C. A. Sanesi, P. A. Dennery, and D. K. Stevenson, "Simultaneous production of carbon monoxide and thiobarbituric acid reactive substances in rat tissue preparations by an iron-ascorbate system," *Canadian Journal of Physiology and Pharmacology*, vol. 76, no. 12, pp. 1057–1065, 1998.

[32] S. Hakomori, "Carbohydrate-to-carbohydrate interaction, through glycosynapse, as a basis of cell recognition and membrane organization," *Glycoconjugate Journal*, vol. 21, no. 3/4, pp. 125–137, 2004.

[33] R. L. Schnaar, "Glycolipid-mediated cell–cell recognition in inflammation and nerve regeneration," *Archives of Biochemistry and Biophysics*, vol. 426, no. 2, pp. 163–172, 2004.

[34] I. Pascher, M. Lundmark, P. G. Nyholm, and S. Sundell, "Crystal structures of membrane lipids," *Biochimica et Biophysica Acta (BBA) - Reviews on Biomembranes*, vol. 1113, no. 3-4, pp. 339–373, 1992.

[35] R. K. Yu, Y. T. Tsai, and T. Ariga, "Functional roles of gangliosides in neurodevelopment: an overview of recent advances," *Neurochemical Research*, vol. 37, no. 6, pp. 1230–1244, 2012.

[36] S. Hakomori, "Structure, organization, and function of glycosphingolipids in membrane," *Current Opinion in Hematology*, vol. 10, no. 1, pp. 16–24, 2003.

[37] M. Bektas and S. Spiegel, "Glycosphingolipids and cell death," *Glycoconjugate Journal*, vol. 20, no. 1, pp. 39–47, 2004.

[38] S. Ngamukote, M. Yanagisawa, T. Ariga, S. Ando, and R. K. Yu, "Developmental changes of glycosphingolipids and expression of glycogenes in mouse brains," *Journal of Neurochemistry*, vol. 103, no. 6, pp. 2327–2341, 2007.

[39] Y. H. Xu, S. Barnes, Y. Sun, and G. A. Grabowski, "Multisystem disorders of glycosphingolipid and ganglioside metabolism," *Journal of Lipid Research*, vol. 51, no. 7, pp. 1643–1675, 2010.

[40] S. Lobasso, P. Tanzarella, D. Vergara, M. Maffia, T. Cocco, and A. Corcelli, "Lipid profiling of *parkin*-mutant human skin

fibroblasts," *Journal of Cellular Physiology*, vol. 232, no. 12, pp. 3540–3551, 2017.

[41] A. Ishii, T. Ikeda, S. Hitoshi et al., "Developmental changes in the expression of glycogenes and the content of N-glycans in the mouse cerebral cortex," *Glycobiology*, vol. 17, no. 3, pp. 261–276, 2007.

[42] Y. Suzuki, M. Yanagisawa, T. Ariga, and R. K. Yu, "Histone acetylation-mediated glycosyltransferase gene regulation in mouse brain during development," *Journal of Neurochemistry*, vol. 116, no. 5, pp. 874–880, 2011.

[43] A. Yamamoto, M. Haraguchi, S. Yamashiro et al., "Heterogeneity in the expression pattern of two ganglioside synthase genes during mouse brain development," *Journal of Neurochemistry*, vol. 66, no. 1, pp. 26–34, 1996.

[44] H. Dreyfus, B. Guérold, L. Freysz, and D. Hicks, "Successive isolation and separation of the major lipid fractions including gangliosides from single biological samples," *Analytical Biochemistry*, vol. 249, no. 1, pp. 67–78, 1997.

[45] N. F. Avrova, I. O. Zakharova, V. A. Tyurin, Y. Y. Tyurina, I. A. Gamaley, and I. A. Schepetkin, "Different metabolic effects of ganglioside GM1 in brain synaptosomes and phagocytic cells," *Neurochemical Research*, vol. 27, no. 7/8, pp. 751–759, 2002.

[46] I. A. Vlasova, I. O. Zakharova, T. V. Sokolova, and N. F. Avrova, "Metabolic effects of ganglioside GM1 on PC12 cells at oxidative stress depend on modulation of activity of tyrosine kinase of trk receptor," *Zhurnal Evoliutsionnoĭ Biokhimii i Fiziologii*, vol. 49, no. 1, pp. 15–23, 2013.

[47] M. Gavella, V. Lipovac, R. Rakos, and B. Colak, "Reduction of oxidative changes in human spermatozoa by exogenous gangliosides," *Andrologia*, vol. 37, no. 1, pp. 17–24, 2005.

[48] H. Sohn, Y. S. Kim, H. T. Kim et al., "Ganglioside GM3 is involved in neuronal cell death," *The FASEB Journal*, vol. 20, no. 8, pp. 1248–1250, 2006.

[49] C. García-Ruiz, A. Colell, R. París, and J. C. Fernández-Checa, "Direct interaction of GD3 ganglioside with mitochondria generates reactive oxygen species followed by mitochondrial permeability transition, cytochrome *c* release, and caspase activation," *The FASEB Journal*, vol. 14, no. 7, pp. 847–858, 2000.

[50] M. R. Rippo, F. Malisan, L. Ravagnan et al., "GD3 ganglioside directly targets mitochondria in a bcl-2-controlled fashion," *The FASEB Journal*, vol. 14, no. 13, pp. 2047–2054, 2000.

[51] M. R. Rippo, F. Malisan, L. Ravagnan et al., "GD3 ganglioside as an intracellular mediator of apoptosis," *European Cytokine Network*, vol. 11, no. 3, pp. 487-488, 2000.

[52] P. Matarrese, T. Garofalo, V. Manganelli et al., "Evidence for the involvement of GD3 ganglioside in autophagosome formation and maturation," *Autophagy*, vol. 10, no. 5, pp. 750–765, 2014.

[53] F. Malisan and R. Testi, "The ganglioside GD3 as the Greek goddess Hecate: several faces turned towards as many directions," *IUBMB Life*, vol. 57, no. 7, pp. 477–482, 2005.

[54] A. Dhanushkodi and M. P. McDonald, "Intracranial *V. cholerae* sialidase protects against excitotoxic neurodegeneration," *PLoS One*, vol. 6, no. 12, article e29285, 2011.

[55] L. Fuentes-Broto, E. Martínez-Ballarín, J. Miana-Mena et al., "Lipid and protein oxidation in hepatic homogenates and cell membranes exposed to bile acids," *Free Radical Research*, vol. 43, no. 11, pp. 1080–1089, 2009.

[56] L. Vitek and J. Ostrow, "Bilirubin chemistry and metabolism; harmful and protective aspects," *Current Pharmaceutical Design*, vol. 15, no. 25, pp. 2869–2883, 2009.

[57] V. Tripodi, M. Contin, M. A. Fernández, and A. Lemberg, "Bile acids content in brain of common duct ligated rats," *Annals of Hepatology*, vol. 11, no. 6, pp. 930–934, 2012.

[58] M. McMillin and S. DeMorrow, "Effects of bile acids on neurological function and disease," *The FASEB Journal*, vol. 30, no. 11, pp. 3658–3668, 2016.

[59] K. L. Mertens, A. Kalsbeek, M. R. Soeters, and H. M. Eggink, "Bile acid signaling pathways from the enterohepatic circulation to the central nervous system," *Front Neurosci*, vol. 11, p. 617, 2017.

[60] Y. P. Rao, R. T. Stravitz, Z. R. Vlahcevic, E. C. Gurley, J. J. Sando, and P. B. Hylemon, "Activation of protein kinase C alpha and delta by bile acids: correlation with bile acid structure and diacylglycerol formation," *Journal of Lipid Research*, vol. 38, no. 12, pp. 2446–2454, 1997.

[61] S. F. Steinberg, "Mechanisms for redox-regulation of protein kinase C," *Front Pharmacol*, vol. 6, p. 128, 2015.

[62] D. Kreutter, J. Y. Kim, J. R. Goldenring et al., "Regulation of protein kinase C activity by gangliosides," *Journal of Biological Chemistry*, vol. 262, no. 4, pp. 1633–1637, 1987.

[63] X. J. Xia, X. B. Gu, A. C. Sartorelli, and R. K. Yu, "Effects of inducers of differentiation on protein kinase C and CMP-N-acetylneuraminic acid:lactosylceramide sialyltransferase activities of HL-60 leukemia cells," *Journal of Lipid Research*, vol. 30, no. 2, pp. 181–188, 1989.

[64] J. Aguilera, C. Padrós-Giralt, W. H. Habig, and E. Yavin, "GT1b ganglioside prevents tetanus toxin-induced protein kinase C activation and down-regulation in the neonatal brain in vivo," *Journal of Neurochemistry*, vol. 60, no. 2, pp. 709–713, 1993.

[65] R. K. Yu and E. Bieberich, "Regulation of glycosyltransferases in ganglioside biosynthesis by phosphorylation and dephosphorylation," *Molecular and Cellular Endocrinology*, vol. 177, no. 1-2, pp. 19–24, 2001.

[66] T. W. Chung, H. J. Choi, Y. C. Lee, and C. H. Kim, "Molecular mechanism for transcriptional activation of ganglioside GM3 synthase and its function in differentiation of HL-60 cells," *Glycobiology*, vol. 15, no. 3, pp. 233–244, 2005.

CLINICAL CHEMISTRY ARTICLE – AUTOMATION AND ANALYTICAL TECHNIQUES (AAT)

Novel accurate quantitative LC-MS/MS method for lumirubin determination

Jana Jašprová[1$], Aleš Dvořák[1$], Marek Vecka[1], Martin Leníček[1], Ondřej Lacina[2], Petra Valášková[1], Miloš Zapadlo[3], Richard Plavka[3], *Libor Vítek[1,4]

[$]Both authors contributed equally

[1]Institute of Medical Biochemistry and Laboratory Diagnostics, 1st Faculty of Medicine, Prague, Charles University, Czech Republic

[2]HPST, s.r.o., Prague, Czech Republic

[3]Department of Paediatrics and Neonatology, Faculty of Medicine, Charles University, Prague, Czech Republic

[4]4th Department of Internal Medicine, 1st Faculty of Medicine, Charles University, Prague, Czech Republic

*Correspondence to:

Libor Vítek, MD, PhD

Institute of Medical Biochemistry and Laboratory Diagnostics

1st Faculty of Medicine, Charles University in Prague

Na Bojišti 3

Praha 2, 12000

Czech Republic

Tel: +420 2 2496 4203

Fax: +420 2 2496 4203

E-mail: vitek@cesnet.cz

Abstract

Background: Phototherapy (PT) represents a standard treatment option for neonatal jaundice. However, no validated clinical method for determination of bilirubin photooxidation products is currently available. Thus, the aim of our study was to establish such method for use in routine clinical chemistry.

Methods: A LC-MS/MS assay for simultaneous determination of lumirubin (the major bilirubin photo-oxidation product) and bilirubin was conducted, using mesobilirubin as an internal standard. Lumirubin was prepared by photo-irradiation of bilirubin and purified by thin layer chromatography. The assay was tested on human sera from neonates treated with standard phototherapy.

Results: Samples were separated on HPLC system with Poroshell 120 EC-C18 column using a binary mobile phase system (NH_4F in water/ CH_3OH) and the analytes were detected in triple quadrupole mass spectrometer operating in a positive SRM mode. The method was linear up to 400 μmol/L for bilirubin and to 100 μmol/L for lumirubin with submicromolar limits of detection, with validity parameters relevant for use in clinical chemistry. Exposure of newborns on phototherapy raised serum lumirubin concentrations three-fold ($p<0.01$), but the absolute concentration was surprisingly low (6.4±2.9 μmol/L), despite dramatic decrease of serum bilirubin concentrations (232.6±41.2 *vs.* 176.0±58.1 μmol/L, $p<0.01$) suggesting formation of additional bilirubin photo-oxidation products as well as presumable increased urinary and biliary secretion of these polar products.

Conclusions: A LC-MS/MS method for the simultaneous determination of lumirubin and bilirubin in human serum was established and validated for use in clinical practice. This method should help to monitor neonates on phototherapy, as well as to help our understanding of kinetics and biology of bilirubin photooxidation products. **Key words:** bilirubin, lumirubin, neonatal jaundice, LC-MS/MS

Introduction

Neonatal jaundice is commonly present in the newborn period. In fact, virtually all newborn infants develop hyperbilirubinemia (>17 μmol/L, 1 mg/dL) during the first week of life. In more than 5 to 31% of neonates the total serum bilirubin concentrations exceed 220 μmol/L (13 mg/dL) depending on geographical region as well as ethnicity (the incidence being lower in blacks and the highest in Asian infants *(1-4)*. Phototherapy (PT) is the treatment of choice since its discovery in 1950's *(5)*. It is based on exposure of neonates to blue to blue-green light (400 to 520 nm, with the maximum at 460 ± 10 nm) *(6)*. The blue light, in turn, is capable of transforming non-polar bilirubin into more polar derivatives - bilirubin photoisomers (Z-lumirubin being the final product of the photoreaction) and other bilirubin oxidation products (Fig. 1).

Although PT is used worldwide in a routine clinical practice, and in general the method is considered safe for babies *(7)*, certain health concerns have been raised recently on the safety issues of this therapeutic approach, especially in extremely low-birth weight neonates. In fact, increased mortality has

been recently reported in this subset of neonates treated with aggressive phototherapy *(8, 9)*. In addition, very recent report by Auger *et al.* demonstrated increased risk late-onset solid tumors in childhood infants treated with phototherapy in the neonatal period *(10)*, a phenomenon which might be related to DNA damage observed in neonates treated with phototherapy *(11)*.

It seems essential that that there is a desperate need for a robust, accurate and sensitive quantitative analytical method for the determination of bilirubin oxidation products generated during PT. These methods are still lacking, namely because these pigments are not stable enough and their determination requires high level of expertise, and even more importantly, standards of neither bilirubin photoisomers nor its oxidation products are commercially available. In fact, there are only scarce data on their preparation with different purity and yields *(12-15)*.

Up to date, only two HPLC methods for determination of lumirubin have been reported. The first one was developed by McDonagh *et al. (16)* in 1982, however this assay was not quantitative and with limited resolution of separated pigments. The other method was based on the correction of the HPLC chromatogram peak area according to the different relative molar absorption coefficients of bilirubin photoisomers, but the method was not tested neonatal samples. *(17)*. In addition, none of these methods used the pure standards of bilirubin photoisomers.

Therefore, the goal of our study was to establish and validate analytical method capable of *Z*-lumirubin quantification in real neonatal serum samples.

Materials and Methods

Chemicals and reagents

Bilirubin was purchased from Sigma-Aldrich (MO, USA) and was purified according to McDonagh and Assisi *(18)*. Mesobilirubin (MBR) was purchased from Frontier Scientific (UT, USA). Human serum albumin (HSA), and rabbit serum albumin (RSA), chloroform p.a., dimethyl sulfoxide (DMSO) p.a., L-ascorbic acid (99%), 2,6-di-*tert*-butyl-4-methylphenol (BHT) (≥99%), and trifluoroacetic acid (TFA) (99%) were purchased from Sigma (MO, USA). Ammonium acetate p.a. and natrium hydroxide p.a. were from Penta (Czech Republic) as well as another common chemicals.

Methanol for HPLC and LC-MS was from Biosolve chimie SARL (France, LC-MS grade) and ammonium fluoride (LC-MS grade) was from Honeywell (International Inc., Morris Plains, NJ, USA).

Blood samples of neonates with hyperbilirubinemia

The collection and use of blood samples of neonates was approved by Ethical committee of General University Hospital in Prague, Czech Republic with informed consent of parents. Blood samples were taken from ten neonates on PT (at day 1 and/or 3), as well as from five untreated controls.

Lumirubin preparation

Because the light sensitivity of bilirubin and lumirubin, all procedures were carried out under dim light in flasks wrapped in the aluminum foil. The evaporation of samples was performed at vacuum rotary evaporator and under the stream of nitrogen.

For Z-lumirubin preparation, we modified previously described method by *(15)*. Briefly, 2.8 mg of bilirubin was solubilized in 2 mL of 0.1 mol/L NaOH, immediately neutralized with 1 mL of 0.1 mol/L H_3PO_4, and mixed with 7 mL of 660 µmol/L RSA (in PBS). The final concentration of bilirubin was 480 µmol/L. The whole mixture was transferred to Petri dish (10 cm diameter) and was photo-irradiated using Lilly phototherapeutical device (TSE, Czech Republic) for 120 minutes at 70 µW/cm^2/nm corresponding to total irradiance of 2.2 mW/cm^2. Photo-irradiated bilirubin solution was deproteinated with 15 ml (3:1) of 0.1 mol/L ammonium acetate in methanol and vortexed. Following the Folch extraction protocol *(19)*, chloroform (20 mL of chloroform per 20 mL of solution, 1:1) was added and intensively shaken. Then, 10 mL of water was added to this solution, vortexed and centrifuged (10 min, 4,000 RPM, 4 ºC). Lower chloroform phase which contained lumirubin was transferred to the centrifugation tubes and centrifuged at 3,000 x g for 10 minutes to eliminate residual impurities and the chloroform phase was evaporated at 60 °C under the stream of nitrogen in glass vials. The residue was dissolved in 300 µL of methanol and separated by thin layer chromatography on silicagel plates [PLC Silica gel 60, 0.5 mm 20 x 20 cm, Sigma] using a mobile phase chloroform:methanol:water, 40:9:1, v/v/v]. The yellow band corresponding to lumirubin (verified by HPLC according to McDonagh *(16)* and by LC-MS/MS) was scraped out from the plate, extracted by methanol and dried under the stream of nitrogen at 60 °C.

The crude lumirubin was dissolved in HSA (400 µmol/L in PBS) and its concentration was measured spectrophotometrically at 453 nm (Microvolume Spectrophotometer DS 11+, DeNovix, USA) in multiple lumirubin dilutions. The lumirubin molar absorption coefficient was 33,000 mol^{-1}dm^{3}cm^{-1} as described earlier *(15)*.

Preparation of calibrators

lumirubin was diluted with HSA to final concentration 200 µmol/L and mixed with unconjugated bilirubin (UCB) diluted by DMSO in the concentration of 800 µmol/L (1:1, v/v, stock solution). This stock solution was subsequently diluted by HSA to final concentration 0.01, 0.1, 1, 10, 25, 50 and 100 µmol/L lumirubin and 0.04, 0.4, 4, 40, 100, 200 and 400 µmol/L of UCB. All calibration solutions as well as internal standard (ISTD) 5 µmol/L of MBR in DMSO were stored at -80 °C and used within a 3-month period. Ten µL of HSA (point zero) or lumirubin/UCB and 20 µL of ISTD were mixed together and prepared for LC-MS/MS analyses.

Preparation of sample

Ten µL of serum sample was mixed with 20 µL of ISTD. Deproteinization was performed after vortex-mixing of sample with 1 mL methanol containing 0.3% BHT, 0.1% ascorbic acid and 0.5% CH_3COONH_4 with subsequent centrifugation for 40 minutes at 16,000 x g. One hundred µL of the final supernatant was carefully taken and 3 µL were injected into LC-MS/MS platform.

Statistical analysis

Normally distributed data are expressed as mean and standard deviation (SD). Differences between variables were evaluated by the Mann-Whitney Rank Sum test. Differences were considered statistically significant when p-values were <0.05. Statistical analyses were performed using Prism 5.03 software (GraphPad, CA, USA).

Results

LC-MS/MS analysis

Samples were separated on HPLC system (Dionex Ultimate 3000, Dionex Softron GmbH, Germany) equipped with Poroshell 120 EC-C18 column (2.1 µm, 3.0 x 100 mm; Agilent, CA, USA). The binary mobile phase system that consisted of 1 mmol/L NH_4F in water (A) and CH_3OH (B) was used at the flow rate of 0.4 mL/min and column chamber heated to 30 °C. The initial isocratic elution of 40 % of B for 3 minutes was followed by the gradient change to 100 % B over 10 minutes and held for additional 4 minutes. The content of phase B was changed to 60 % in 0.1 minutes (17 →17.1 minutes) and was kept at 60 % till the end of the gradient program at 20 minutes. Then, the content of B phase turned back to 40 % within one minute, followed by 4-minute equilibration time (i.e. total run time 25 minutes). To reduce the contamination of the detector, the flow from HPLC was turned to the detector from 2 to 21 min only.

The analytes were detected in triple quadrupole mass spectrometer (TSQ Quantum Access Max with HESI-II probe, Thermo Fisher Scientific, Inc., USA) operating in positive SRM mode. The heated HESI-II probe for MS detector was run under following conditions: spray voltage +3200 V, vaporizer temperature 350 °C, sheath gas 40 arbitrary units (au), auxiliary valve flow 15 au, ion sweep gas pressure 5.0 au, capillary temperature 320 °C. Skimmer offset voltage was not used. The tuning of MS/MS transitions was performed by combined infusion of analytes (10 mg/L in the mobile phase, 20 µL/min) and the mobile phase (400 µL/min), collision gas (Ar) pressure was set to 1.5 mTorr. Monitored transitions (corresponding collision energy) were as follows: bilirubin [585.3 → 299.1 (20 V); 585.3 → 271.2 (18 V)], lumirubin [585.3 → 299.1 (20 V); 585.3 → 285.1 (18 V)], and MBR [589.3 → 301.1 (20 V); 589.3 → 273.2 (44 V)]. Tube lens voltage was set at 83 V for bilirubin, 112 V for lumirubin, and 85 V for MBR (Fig. 2).

Method validation

Stability

Serum samples, spiked with standards (UCB, lumirubin) at three concentration levels (4, 40 and 400 µM UCB paired with concentrations of lumirubin - 1, 10 and 100 µM), were repeatedly measured during long time period. Each sample was measured 10 times in succession (approximately 1 analysis per half hour). The procedure was as follows: The sample spiked with first concentration level was 10-times injected during 6 hours, then fresh sample of another spiked concentration level was prepared and was measured next 6 hours (also 10 injections). Finally, sample with spiked concentration level 3 was prepared and measured. Every sample was kept at 15 °C in auto-sampler. Very fast degradation of internal standard was observed (The observed intensities of analyte peaks decreased within 2.5 hours) without antioxidants added but the use of antioxidants (BHT, ascorbic acid) improved the stability of internal standard as well as lumirubin and UCB – no significant degradation was observed during the 6-hour testing. Plasma samples for lumirubin analysis can be stored at -80°C for at least three months. Repeated freeze-thawing of the samples is not recommended.

Linearity

Linearity was tested using 8 calibration levels (points???) in triplicates in range 0.04 - 400 µmol/L and 0.01 - 100 µmol/L for UCB and lumirubin, respectively (see Fig. 3).

Limit of detection

Limit of detection was estimated as a concentration corresponding to a signal 3 SD above the mean for a calibrator free of analyte (n=10) and was 100 pmol/L for lumirubin and 80 pmol/L for UCB.

Limit of quantification

Limit of quantification was estimated as a concentration corresponding to a signal 10 SD above the mean for a calibrator free of analyte (n=10) and was 330 pmol/L for lumirubin and 264 pmol/L for UCB. Values of limits of detection and quantification were confirmed by analytical software Qual Browser Thermo Excalibur 2.2 SP1.48, where signal-to-noise ratio was calculated.

Intraassay imprecision

Intraassay imprecision was measured in one day and variation coefficient (CV) for 10 measurements of 3 specimens representing three spiked concentration levels (see Stability assay) was calculated as SD/mean (Tab. 1).

Interassay imprecision

Interassay imprecision was measured over a 2-months period and variation coefficient (CV) for 10 measurements of 3 specimens was calculated (Tab. 1).

Average recovery

The average recovery was calculated as [(measured concentration-initial concentration)/added concentration] for levels of monitored analytes used in assay imprecision (n=10, Tab. 1).

Interference testing

Interferences were estimated as the recovery of a known amount of analyte added to human serum samples containing various interferents (hemolytic, chylous, and hyperbilirubinemic; Tab. 2).

Within **robustness** was tested influence of small procedure changes and no differences were observed – data not shown.

Determination of lumirubin in clinical serum samples

All newborn children developed jaundice during 4 days after the birth, in one case, hyperbilirubinemia was developed already on the day 2. The mean basal concentration of lumirubin was 2.1±1.3 μmol/L in neonates indicated for PT Concentration of lumirubin raised to 6.4±2.9 μmol/L after 1st day of PT (3-fold vs. before PT, $p < 0.01$) On the other hand, UCB concentrations decreased, as expected from the mean concentration of 232.6±41.2 μmol/L before the treatment to 176.0 ± 58.1 (0.76-fold *vs.* before treatment, $p < 0.01$) μmol/L on the day one of PT. (Fig. 4).

Discussion

Although PT became a worldwide used treatment option for neonatal jaundice (and principally replaced former used exchange transfusion *(20)* since its discovery in 1958 *(5)*, it is still a mystery, what concentrations of bilirubin PI could be found in the neonates before, during and after PT. One of several reasons of lacking information about the fate of UCB after PT is the complexity of mammalian body. In general, the binding between albumin and UCB (strength, UCB/albumin ratio) may significantly affect conversion of UCB into its PI. HSA had evolved uniquely to counteract UCB toxicity in brain *(21, 22)*. As it seems, HSA has very specific properties which may directly influence PT success *(23)*. Another but not less important reason is a lack of commercially available standards of bilirubin PI and also of their photolability and instability that makes them hard to work with.

Based on the protocol of McDonagh *(15)* we were previously able to isolate pure standard of lumirubin in quantity high enough for cellular experiments *(24)*. For this study, it was necessary to adapt the method to prepare lumirubin standard in purity high enough for LC-MS/MS analysis. Thus, we modified the recently described procedure *(24)* and added a step of the extraction of lumirubin into chloroform which helped us to isolate higher amount of lumirubin pure enough for LC-MS/MS tuning (and for LC-MS calibrators). After preparative method development and after LC-MS/MS tuning we focused on LC-MS/MS validation.

Previously, one qualitative *(16)* and one quantitative method *(17)* was published, but none of them was suitable for LC-MS/MS analysis due to solvents used, which were not compatible for use with MS detectors. Moreover, no internal standards were used in these methods questioning thus their reliability. In presented study, we validated as the first group, the accurate, sensitive LC-MS/MS method for the determination of the major bilirubin PI, lumirubin, together with UCB in the serum of neonates with hyperbilirubinemia.

Validation of the method was divided into the several steps according Leníček *et al. (25)*. The most important attribute of the whole validation procedure was stability of all analytes (including internal standard). It was found out that all samples could be stored at -80 °C for long time period (at least 3 months) but during preparation and analysis they could be degraded very fast. Moreover, without the usage of any additives (antioxidants) the ratio of BR or lumirubin to ISTD was changed within six hours of analysis and analytes degraded completely after 12 – 24 hours. For the analysis by autosampler, it was necessary to find out optimal cocktail of antioxidants, strong enough to protect the samples.

Concentrations and ratio of BHT and ascorbic acid (vitamin C alone degrades in a few hours) were used as described previously *(26, 27)* and experimentally modified for our conditions. These two additives allowed much longer analysis time and more important the ratio between analytes and ISTD stayed the same during the whole sequence of measurements.

Imprecisions of the whole procedure were evaluated by three parameters – Intra/Inter-assay imprecision and Average recovery – and were expressed as a CV. Our results suggest relatively small mistakes (with respect to the instability of the analytes), but Zelenka *et al. (28)* observed much lower imprecisions during validation of UCB analysis by HPLC. Probably the main reason was the absence of MS detector which may bring another mistake caused by ionization. It is necessary to take into account this fact during evaluating of inter-assay imprecision and other parameters after LC-MS/MS analysis. Final step of validation was to measure interferences. Fortunately, recoveries data have not indicated any dramatic influences of matrix and method is usable for clinical samples.

We have no doubts about beneficial effects of phototherapy in lowering high dangerous levels of bilirubin in neonates with hyperbilirubinemia. There are only rare papers pointing the side effects of the treatment *(29)*. However, studies in neonates with extreme low birth weight *(8, 9, 30)* showed that intensive phototherapy in this group could be accompanied with higher risk of morbidity and mortality. Moreover, in our previous studies we did not find the effect of bilirubin PI on the viability of neuronal cells *(24)*, however, lumirubin might have potential neuro-inflammatory effects as demonstrated by increased production of pro-inflammatory cytokines in *in vitro* and *ex vivo* experimental models of neuronal tissue *(31)*. Despite, it is really important to have a reliable analytical tool for the determination of lumirubin in neonates undergoing PT.

In the recent paper of Ebbesen *et al. (32)*, they adapted HPLC method of Itoh *et al. (17)* to demonstrate levels of lumirubin in two groups of neonates before and 24 h after the PT treated with the light of two different wavelengths (497 and 459 nm). However, lumirubin levels before PT in their paper were significantly lower than in our experiments [0.3 (0.1-0.5) μmol/L and 0.3 (0.2-0.7) μmol/L for the light 497 and 459 nm, respectively, vs. 1.7±0.4 μmol/L or 2.1±1.3 μmol/L in our control or treated group, respectively]. lumirubin values in neonates undergoing 24 h of PT in their study [2.5 (2.2-2.8) μmol/L and 2.1 (1.6-2.5) μmol/L for 497 and 459 nm] were also lower than in our samples (6.4±2.9 μmol/L and 3.6±2.3 μmol/L on the first or second day of PT, respectively), moreover similar to lumirubin levels that we measured before PT (2.1±1.3 μmol/L).

References

1. Bhutani VK, Gourley GR, Adler S, Kreamer B, Dalin C, Johnson LH. Noninvasive measurement of total serum bilirubin in a multiracial predischarge newborn population to assess the risk of severe hyperbilirubinemia. Pediatrics 2000;106:E17.
2. Maisels MJ, Fanaroff AA, Stevenson DK, Young BW, Vreman HJ. Serum bilirubin levels in an international, multiracial newborn population. Ped Res 1999;45:167a-a.
3. Fouzas S, Mantagou L, Skylogianni E, Mantagos S, Varvarigou A. Transcutaneous bilirubin levels for the first 120 postnatal hours in healthy neonates. Pediatrics 2010;125:e52-7.
4. Newman TB, Easterling MJ, Goldman ES, Stevenson DK. Laboratory evaluation of jaundice in newborns; frequency,cost, yield. Am J Dis Child 1990;144:364-8.
5. Cremer RJ, Perryman PW, Richards DH. Influence of light on the hyperbilirubinemia of infants. Lancet 1958;i:1094-7.
6. Vreman HJ, Wong RJ, Stevenson DK. Phototherapy: Current methods and future directions. Semin Perinatol 2004;28:326-33.
7. Maisels MJ, McDonagh AF. Phototherapy for neonatal jaundice. N Engl J Med 2008;358:920-8.
8. Tyson JE, Pedroza C, Langer J, Green C, Morris B, Stevenson D, et al. Does aggressive phototherapy increase mortality while decreasing profound impairment among the smallest and sickest newborns? J Perinatol 2012;32:677-84.
9. Arnold C, Pedroza C, Tyson JE. Phototherapy in elbw newborns: Does it work? Is it safe? The evidence from randomized clinical trials. Semin Perinatol 2014;38:452-64.
10. Auger N, Laverdiere C, Ayoub A, Lo E, Luu TM. Neonatal phototherapy and future risk of childhood cancer. Int J Cancer 2019.
11. Ramy N, Ghany EA, Alsharany W, Nada A, Darwish RK, Rabie WA, Aly H. Jaundice, phototherapy and DNA damage in full-term neonates. J Perinatol 2016;36:132-6.
12. Bonnett R, Buckley DG, Hamzetash D, Hawkes GE, Ioannou S, Stoll MS. Photobilirubin ii. Biochem J 1984;219:1053-6.
13. Stoll MS, Vicker N, Gray CH, Bonnett R. Concerning the structure of photobilirubin ii. Biochem J 1982;201:179-88.
14. Stoll MS, Zenone EA, Ostrow JD, Zarembo JE. Preparation and properties of bilirubin photoisomers. Biochem J 1979;183:139-46.

15. McDonagh AF. Bilirubin photo-isomers: Regiospecific acyl glucuronidation in vivo. Monatsh Chem 2014;145:465-82.
16. McDonagh AF, Palma LA, Trull FR, Lightner DA. Phototherapy for neonatal jaundice. Configurational isomers of bilirubin. J Am Chem Soc 1982;104:6865-9.
17. Itoh S, Isobe K, Onishi S. Accurate and sensitive high-performance liquid chromatographic method for geometrical and structural photoisomers of bilirubin ix alpha using the relative molar absorptivity values. J Chromatogr A 1999;848:169-77.
18. McDonagh AF, Assisi F. The ready isomerization of bilirubin ix- in aqueous solution. Biochem J 1972;129:797-800.
19. Folch J, Lees M, Stanley GHS. A simple method for the isolation and purification of total lipides from animal tissues. J Biol Chem 1957;226:497-509.
20. Drew JH, Marriage K, Bayle VV, Bajraszewski E, McNammara JM. Phototherapy. Short and long-term complications. Arch Dis Child 1976;51:454-8.
21. Itoh S, Onishi S. Kinetic study of the photochemical changes of (zz)-bilirubin ix alpha bound to human serum albumin. Demonstration of (ez)-bilirubin ix alpha as an intermediate in photochemical changes from (zz)-bilirubin ix alpha to (ez)-cyclobilirubin ix alpha. Biochem J 1985;226:251-8.
22. Onishi S, Itoh S, Yamakawa T, Isobe K, Manabe M, Toyota S, Imai T. Comparison of kinetic study of the photochemical changes of (zz)- bilirubin ix alpha bound to human serum albumin with that bound to rat serum albumin. Biochem J 1985;230:561-7.
23. Iwase T, Kusaka T, Itoh S. (ez)-cyclobilirubin formation from bilirubin in complex with serum albumin derived from various species. J Photochem Photobiol B 2010;98:138-43.
24. Jasprova J, Dal Ben M, Vianello E, Goncharova I, Urbanova M, Vyroubalova K, et al. The biological effects of bilirubin photoisomers. PLoS One 2016;11:e0148126.
25. Lenicek M, Juklova M, Zelenka J, Kovar J, Lukas M, Bortlik M, Vitek L. Improved hplc analysis of serum 7alpha-hydroxycholest-4-en-3-one, a marker of bile acid malabsorption. Clin Chem 2008;54:1087-8.
26. Soares DG, Andreazza AC, Salvador M. Sequestering ability of butylated hydroxytoluene, propyl gallate, resveratrol, and vitamins c and e against abts, dpph, and hydroxyl free radicals in chemical and biological systems. J Agric Food Chem 2003;51:1077-80.

27. Reddy AC, Lokesh BR. Studies on spice principles as antioxidants in the inhibition of lipid peroxidation of rat liver microsomes. Mol Cell Biochem 1992;111:117-24.

28. Zelenka J, Lenicek M, Muchova L, Jirsa M, Kudla M, Balaz P, et al. Highly sensitive method for quantitative determination of bilirubin in biological fluids and tissues. Journal of chromatography B, Analytical technologies in the biomedical and life sciences 2008;867:37-42.

29. Xiong T, Qu Y, Cambier S, Mu D. The side effects of phototherapy for neonatal jaundice: What do we know? What should we do? Eur J Pediatr 2011;170:1247-55.

30. Morris BH, Oh W, Tyson JE, Stevenson DK, Phelps DL, O'Shea TM, et al. Aggressive vs. Conservative phototherapy for infants with extremely low birth weight. N Engl J Med 2008;359:1885-96.

31. Jašprová J, Dal Ben M, Hurný D, Hwang S, Žížalová K, Kotek J, et al. Neuro-inflammatory effects of photodegradative products of bilirubin. Scientific reports 2018;8:7444.

32. Ebbesen F, Madsen PH, Vandborg PK, Jakobsen LH, Trydal T, Vreman HJ. Bilirubin isomer distribution in jaundiced neonates during phototherapy with led light centered at 497 nm (turquoise) vs. 459 nm (blue). Pediatr Res 2016;80:511-5.

Table 1. Intraassay imprecision, interassay imprecision and average recovery in clinically relevant UCB and lumirubin concentrations.

Bilirubin [µmol/L]	**Intraassay Imprecision** CV [%]	**Interassay imprecision** CV [%]	**Average recovery** AC ± SD [%]
4	11	25	118± 30
40	18	20	108 ± 20
400	6.5	9.9	101 ± 5
Lumirubin [µmol/L]			
1	13	21	93 ± 32
10	14	29	78 ± 12
100	15	27	101 ± 4

AC, average recovery; CV, coefficient of variation; SD, standard deviation

Table 2: Recoveries for known concentration of UCB and lumirubin in different matrices

Interferences	**Bilirubin**	**Lumirubin**
Hyperbilirubinemia (50 µmol/L)	132 %	75 %
Hyperbilirubinemia (210 µmol/L)	108 %	72 %
Hypertriacylglycerolemia (2.88 mmol/L)	123 %	120 %
Hypertriacylglycerolemia (>11.3 mmol/L)	113 %	100 %
Hemolytic serum (hemoglobin g/L)	80 %	74 %

Figure Legends

Fig. 1. Bilirubin photo-oxidation products and their fate in human body

Fig. 2. LC-MS/MS chromatograms of standards in biological matrix (serum).

(**A**) LR (10 μM), retention time (RT) = 9.66 min; (**B**) UCB (40 μM), RT = 14.80 min; and (**C**) and MBR (internal standard), RT = 15.04 min are depicted by arrows. Smaller peaks close to RT of bilirubin (14.45 min and 15.11) represent bilirubin´s isomers. A, B and C chromatograms are presented as a TIC summary of two MRM transitions (shown on the right).

LR, lumirubin; UCB, unconjugated bilirubin;, MBR, mesobilirubin.

Fig. 3. Calibration curves of unconjugated bilirubin (UCB) and lumirubin.

I. Calibration curve of UCB. ISTD – internal standard (MBR); **II**. Calibration curve of lumirubin.

Fig. 4. Levels of UCB and lumirubin in neonates before and after PT.

No PT are neonates with neonatal jaundice before PT. ** - $p < 0.01$ (paired-t test).

Fig. 1.

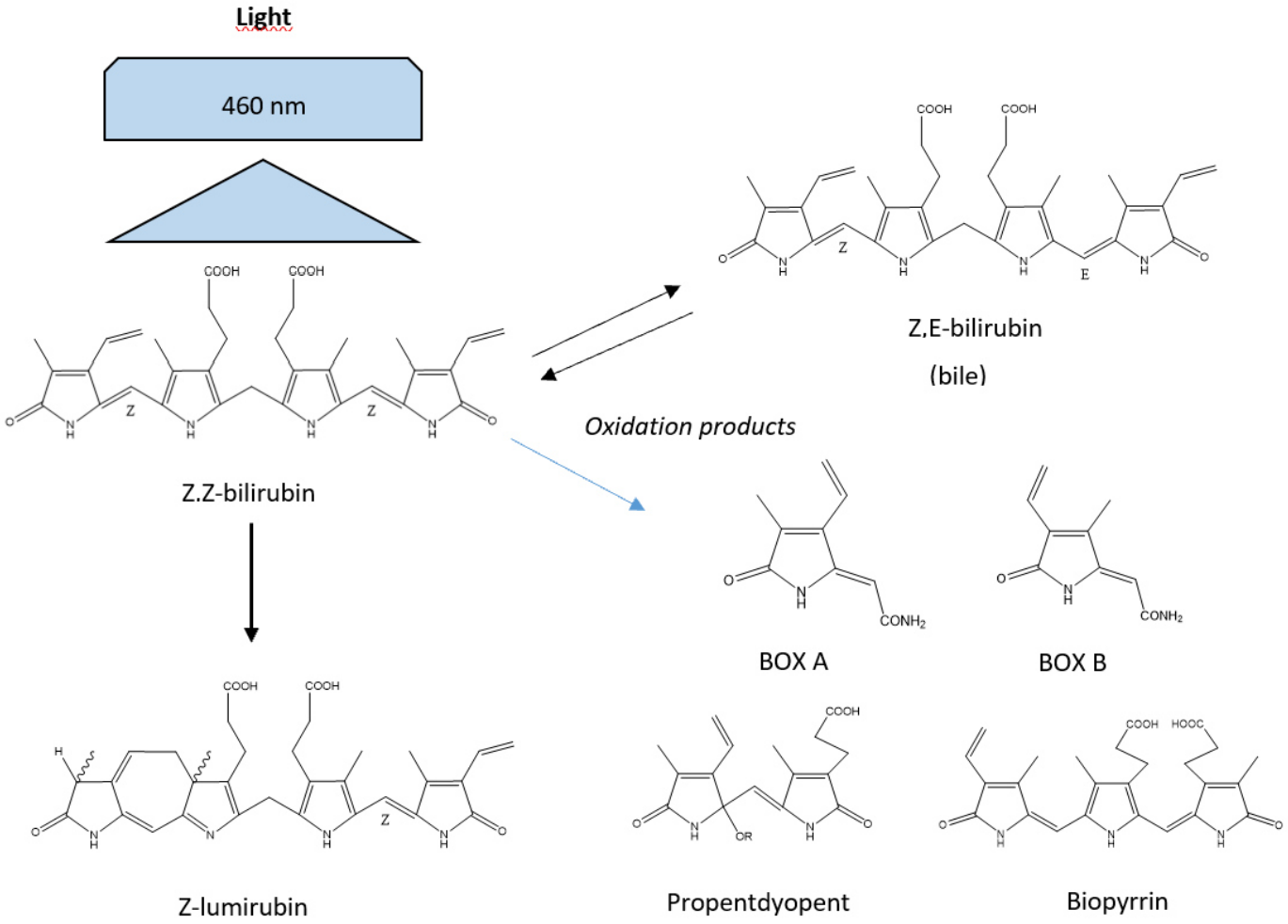
Light
460 nm
Z,E-bilirubin
(bile)
Oxidation products
Z.Z-bilirubin
BOX A
BOX B
Z-lumirubin
Propentdyopent
Biopyrrin

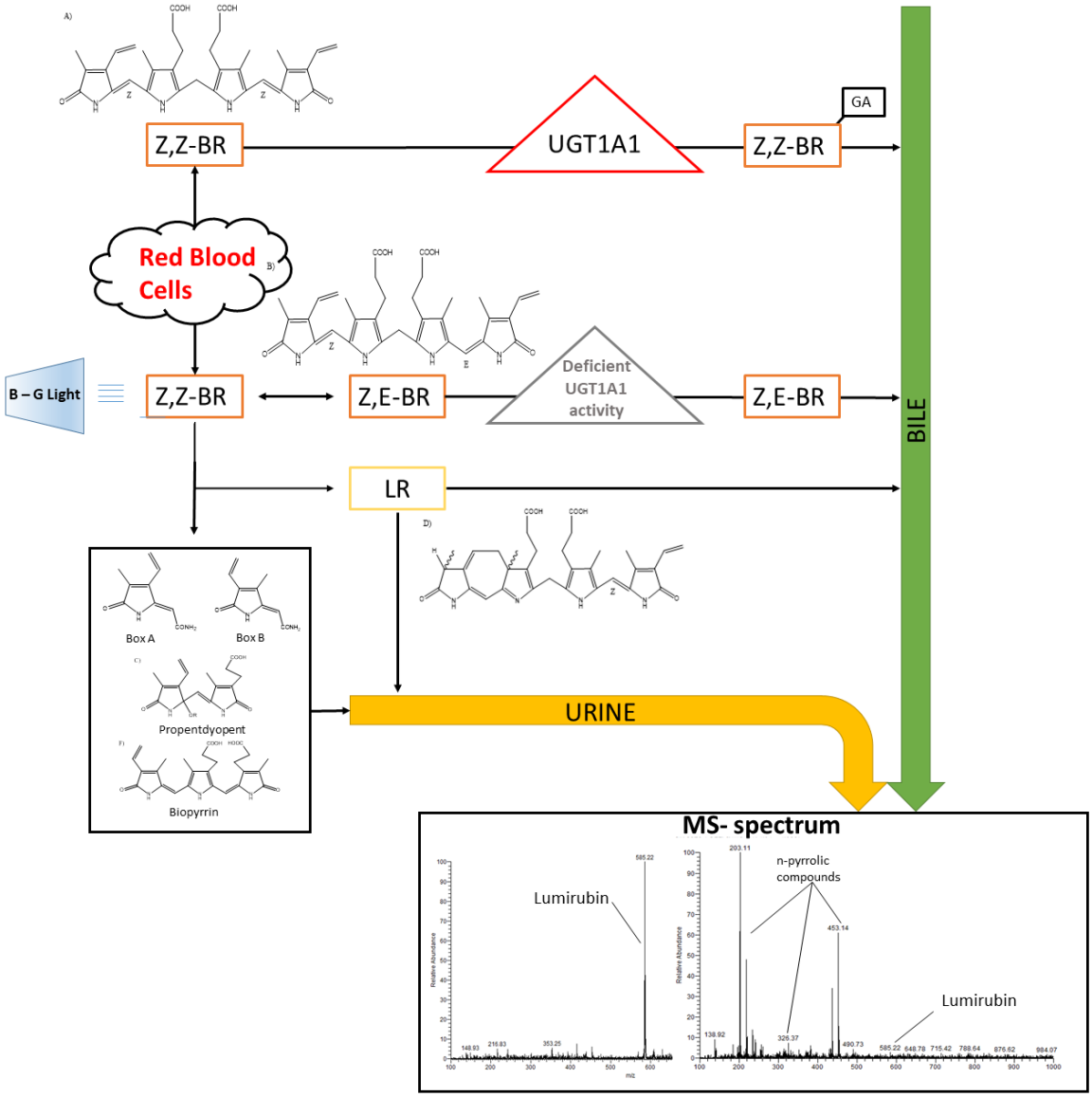
Z,Z-BR
UGT1A1
GA
Z,Z-BR
Red Blood Cells
B – G Light
Z,Z-BR
Z,E-BR
Deficient UGT1A1 activity
Z,E-BR
BILE
LR
Box A
Box B
Propentdyopent
Biopyrrin
URINE
MS- spectrum
Lumirubin
n-pyrrolic compounds
Lumirubin

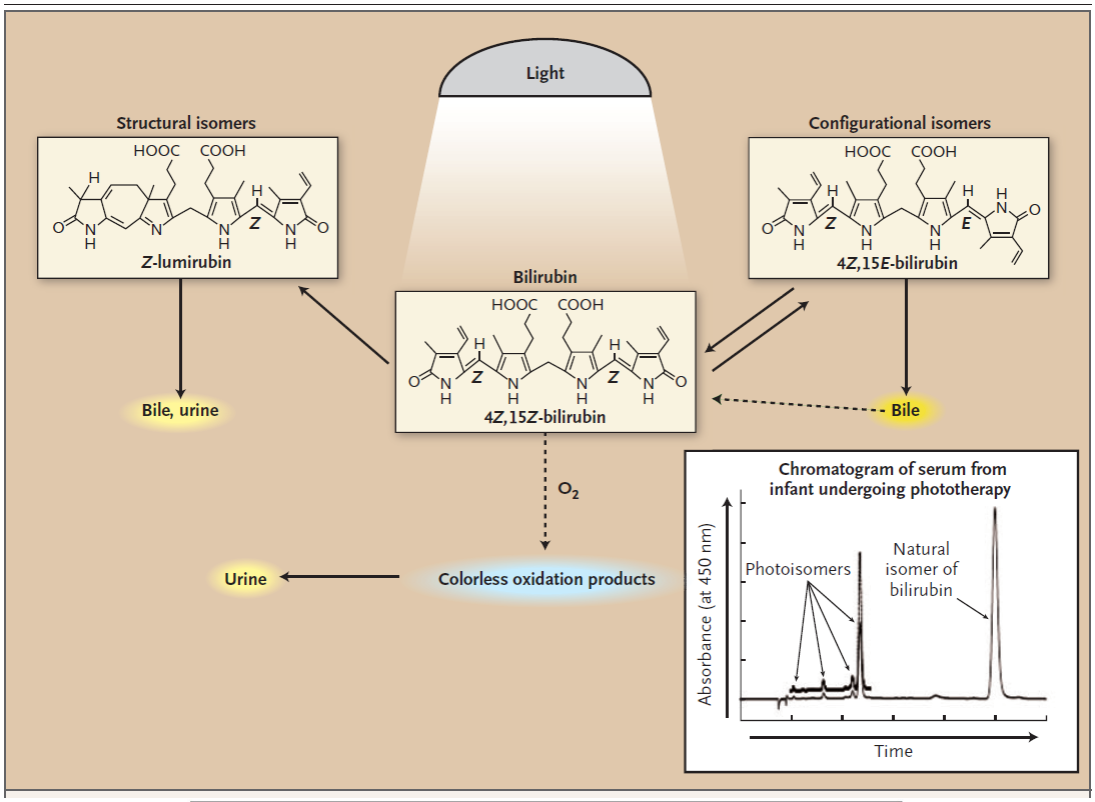
Light
Structural isomers
HOOC COOH
Z-lumirubin
Configurational isomers
HOOC COOH
4Z,15E-bilirubin
Bilirubin
HOOC COOH
4Z,15Z-bilirubin
Bile, urine
Bile
O2
Urine
Colorless oxidation products
Chromatogram of serum from infant undergoing phototherapy
Absorbance (at 450 nm)
Photoisomers
Natural isomer of bilirubin
Time

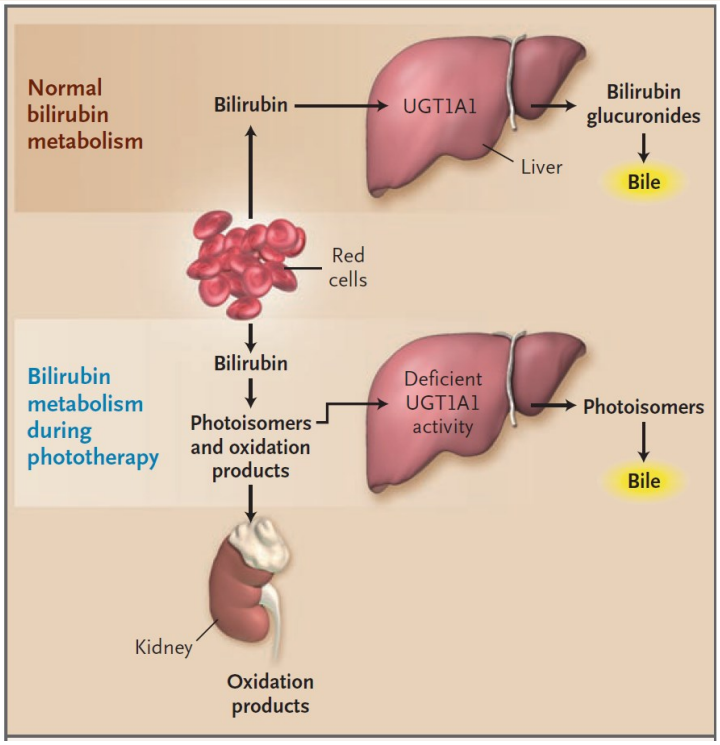
Normal bilirubin metabolism
Bilirubin
UGT1A1
Liver
Bilirubin glucuronides
Bile
Red cells
Bilirubin metabolism during phototherapy
Bilirubin
Photoisomers and oxidation products
Deficient UGT1A1 activity
Photoisomers
Bile
Kidney
Oxidation products

Fig. 2.

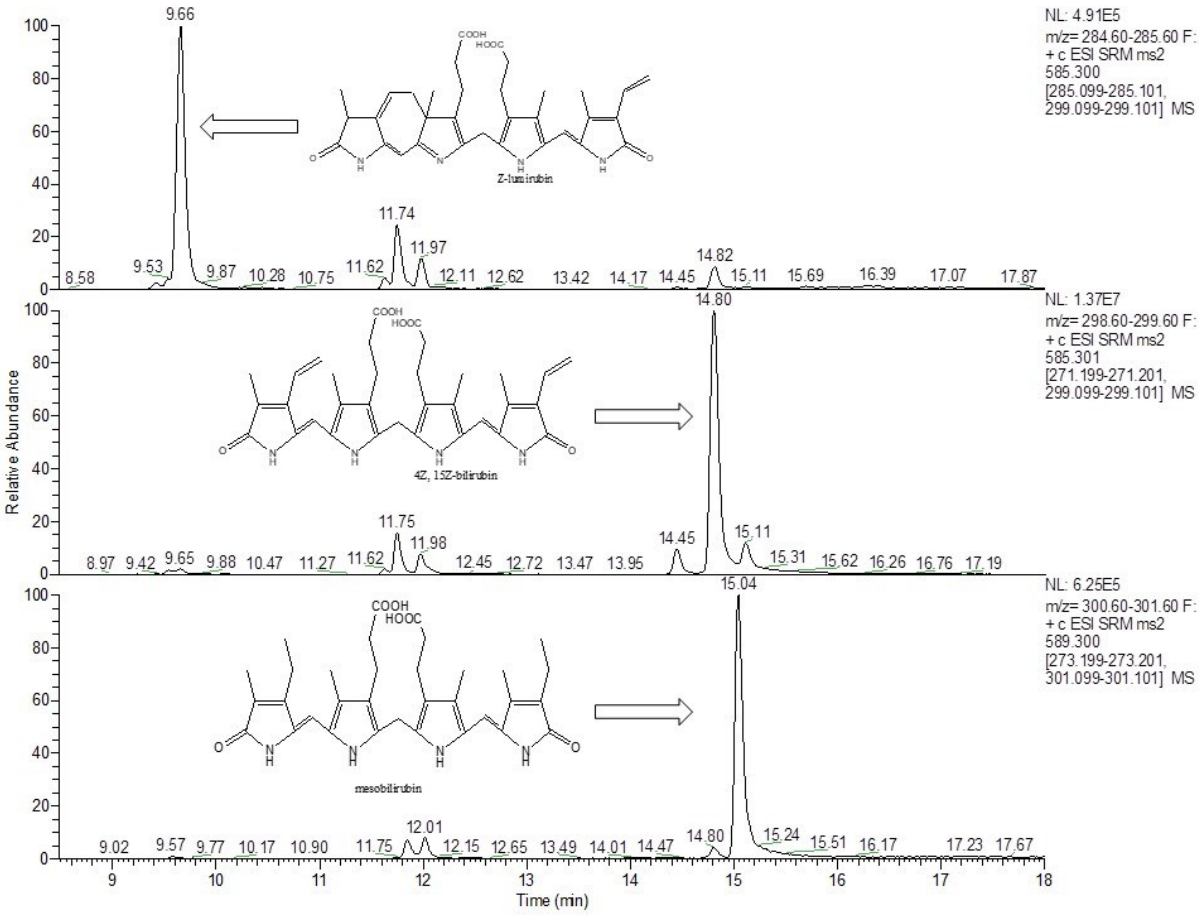
NL: 4.91E5
m/z= 284.60-285.60 F:
+ c ESI SRM ms2
585.300
[285.099-285.101,
299.099-299.101] MS
Z-lumirubin
NL: 1.37E7
m/z= 298.60-299.60 F:
+ c ESI SRM ms2
585.301
[271.199-271.201,
299.099-299.101] MS
4Z, 15Z-bilirubin
NL: 6.25E5
m/z= 300.60-301.60 F:
+ c ESI SRM ms2
589.300
[273.199-273.201,
301.099-301.101] MS
mesobilirubin
Relative Abundance
Time (min)

Fig. 3.

I.

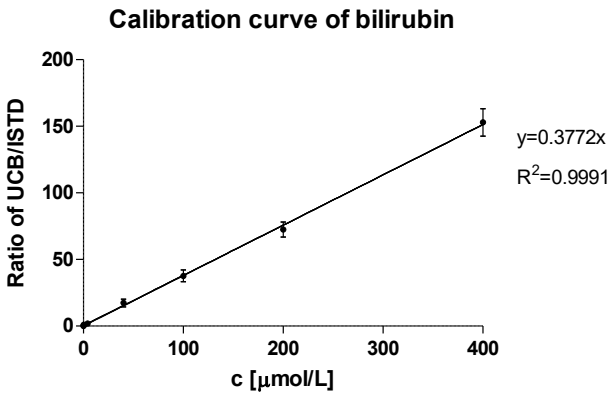
Calibration curve of bilirubin
Ratio of UCB/ISTD
200
150
100
50
0
0
100
200
300
400
c [µmol/L]
y=0.3772x
R2=0.9991

II.

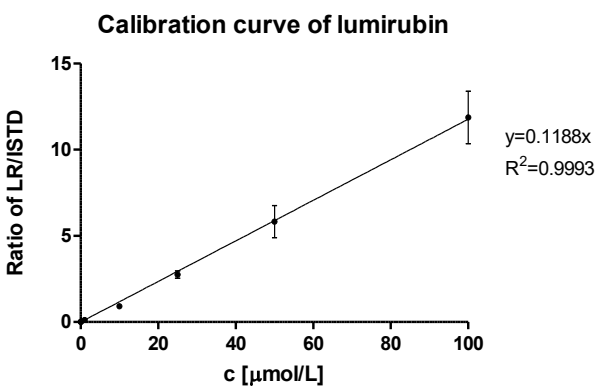
Calibration curve of lumirubin
Ratio of LR/ISTD
15
10
5
0
0
20
40
60
80
100
c [µmol/L]
y=0.1188x
R2=0.9993

Fig. 4.

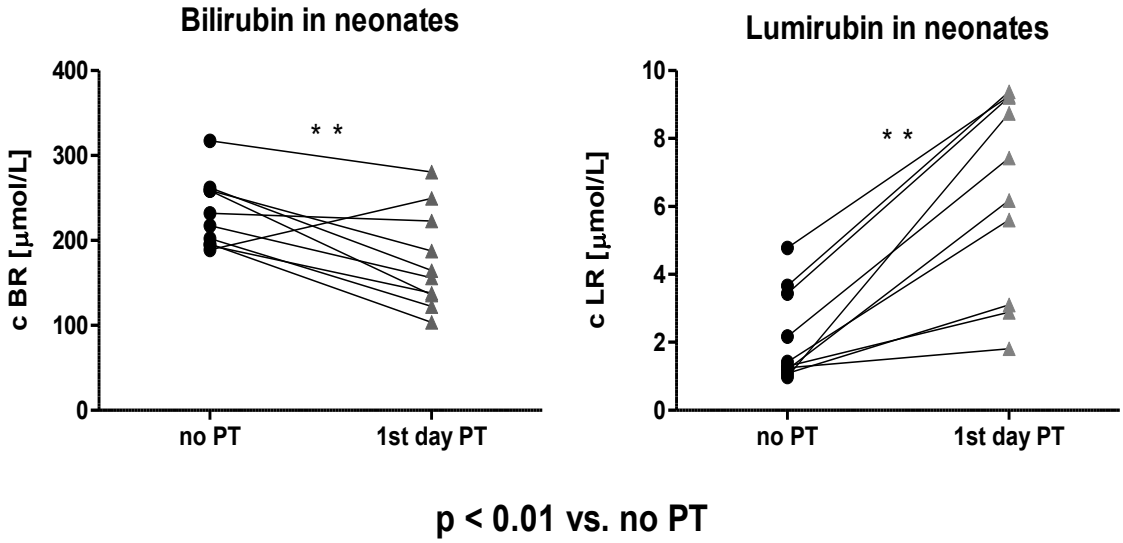

p < 0.01 vs. no PT